Ecological Indicators 159 (2024) 111670

Contents lists available at ScienceDirect

Ecological Indicators

journal homepage: www.elsevier.com/locate/ecolind

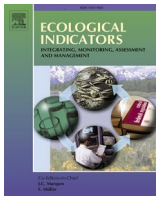

Random forest-based analysis of land cover/land use LCLU dynamics associated with meteorological droughts in the desert ecosystem of Pakistan

Zulqadar Faheem [a], Jamil Hasan Kazmi [a], Saima Shaikh [a], Sana Arshad [b], Noreena [b], Safwan Mohammed [c,d,*]

[a] Department of Geography, University of Karachi, Karachi 75270, Pakistan
[b] Department of Geography, the Islamia University of Bahawalpur, Bahawalpur 63100, Pakistan
[c] Institute of Land Use, Technical and Precision Technology, Faculty of Agricultural and Food Sciences and Environmental Management, University of Debrecen, Debrecen, 4032 Hungary
[d] Institutes for Agricultural Research and Educational Farm, University of Debrecen, Böszörményi 138, 4032 Debrecen, Hungary

ARTICLE INFO

Keywords:
Change Detection
Climate Change
SPI
Development
Arid ecosystem

ABSTRACT

Dry land ecosystems extend over 40 % of the Earth, supporting an estimated 3 billion human population. Thus, quantifying LCLU changes in such ecosystems is essential for achieving sustainable development goals. In this context, this research aimed to examine the LCLU changes in the past three decades (1990 – 2020) in an arid ecosystem of Pakistan, i.e., the Cholisatn desert. Three remote sensing indices, the normalized difference vegetation index (NDVI), normalized difference barren index (NDBaI), and top grain soil index (TGSI) are taken as LCLU representatives to examine their temporal relationship associated with meteorological drought, e.g. the standardized precipitation index (SPI). Moreover, machine learning-based random forest (RF) classification followed by change detection techniques was implemented. Results from RF classifier revealed the applicability of RF in accurately predicting LULC with validation overall accuracy of 0.99. Output of the research revealed an interesting finding where the desert experienced significant LCLU change over the last three decades. The highest vegetation expansion (4.4 %) took place from 2014 to 2020 at the expense of the highest reduction of barren land (-6.3 %). Mann-Kendall trend (MK) and Sen's slope (SS) analysis showed a significant ($P < 0.001$) increasing trend of NDVI (SS = 0.004), SPI (SS = 0.01 and 0.04) and decreasing trend of NDBaI and TGSI (SS = -0.001, −0.005). Interestingly, the significant positive Pearson correlation range (r = 0.6–0.8) of NDVI with SPI-1 to 6, and negative correlation range (r = 0.5–0.7) of NDBaI with SPI indices reveals a strong linear relationship between LCLU and meteorological drought. The research provides substantial implications for policy makers and stakeholders emphasizing the need for proactive strategies such as drought resistant vegetation to improve and maintain the ecological health of desert and combating the negative impacts of climatic change.

1. Introduction

Drylands or deserts are a significant part of terrestrial ecosystems modified by a range of climatic factors and human activities (Martínez-Valderrama et al., 2020; McCluney et al., 2012). Dryland encompasses approximately 40 % land area of the terrestrial Earth with an estimated 3 billion human population by 2020 (Biazin and Sterk, 2013; Burrell et al., 2020). They are comprehended by below-average precipitation and a high rate of evapotranspiration with less potential for soil moisture causing self-propagating drought condition (Schumacher et al., 2022). Hence, the surface water index (SWI), *i.e.*, the ratio of annual precipitation and potential evapotranspiration below 0.65 defines the desert ecosystem appropriately (Yang et al., 2017). Around 18 million sq. km of land in Asia is occupied by dry or deserted regions with rangeland, arable land, forest, and urban area as major land use of the region (Biazin and Sterk, 2013). Several land use changes in desert ecosystems like intensification of agriculture and urban expansion are taking place at the expense of rangeland (Halmy et al., 2015). A previous study by Ge et al. (2022) addressed the changes in ecosystem services associated with LCLU in a desert ecotone of China. For instance, a recent study by Wang et al. (2024) predicted the impacts of human induced land use changes on the soil crust distribution of drylands in China.

* Corresponding author.
E-mail address: safwan@agr.unideb.hu (S. Mohammed).

https://doi.org/10.1016/j.ecolind.2024.111670
Received 31 May 2023; Received in revised form 16 January 2024; Accepted 29 January 2024
Available online 3 February 2024

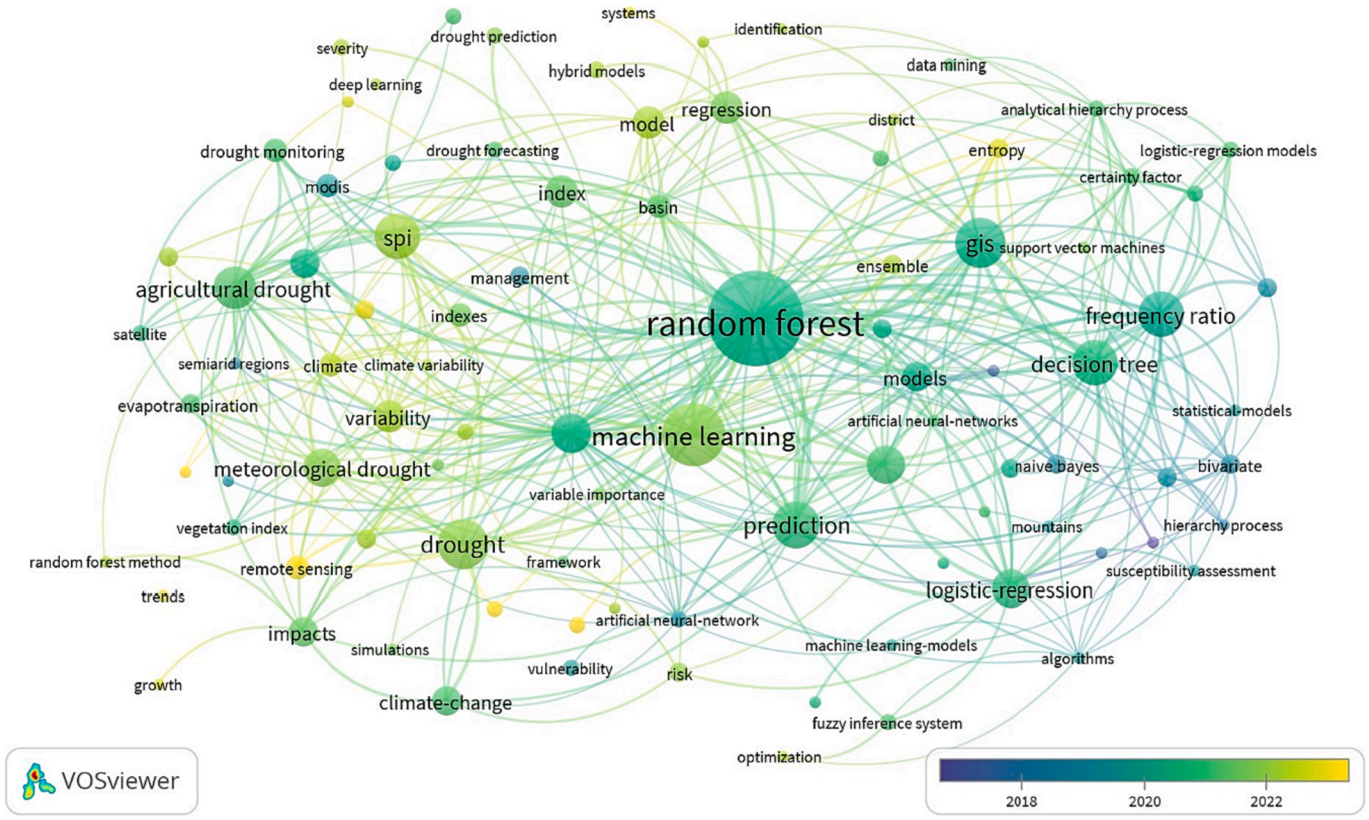

Fig. 1. A Bibliographic Review of Research Related to the Topic in Web of Science, Visualized Using VOSviewer.

Similarly, Zhao et al. (2024) also demonstrated that approximate 50 % of greening trend of drylands of China are attributed to combined effects of land use change and climate processes. LCLU of the deserted regions is mostly associated with several climatic factors like temperature, rainfall, and CO_2 level (Wang et al., 2023). Studies of arid regions have reported an increase in greenness positively associated with precipitation at the global and regional scale (Fensholt et al., 2012; He et al., 2019). On the contrary, it is also reported that global drylands experienced a noticeable decrease in greenness and an increase in barrenness at a certain period due to extreme temperature and below-average precipitation (Burrell et al., 2020; He et al., 2023; Schulz et al., 2010). Further, CO_2 increase is also found to be correlated with soil moisture content and vegetation dynamics of the global dryland ecosystem (Lu et al., 2016). However, the influence of climatic factors in deriving the LCLU changes varies from region to region. For example, the drylands of central Asia are mostly dependent on variations in temperature and high rate of evapotranspiration (Daramola and Xu, 2022). For instance, Fu et al. (2017) also reported that drying and warming trend in the central Asian arid region fostered the wind erosion and reduced the water holding capacity and agricultural expansion. Moreover, human activities like crop production and socioeconomic and infrastructure development are also causing significant changes in LCLU of dry arid regions (Rasmussen et al., 2012). Due to population growth, drylands of developing countries are more closely affected by expansion and intensification of agriculture to meet the increasing food demands (Kleemann et al., 2017). The most noticeable land use change in drylands is the conversion to agricultural or cropland mostly occurring in developing countries of Asia (Song et al., 2018).

In the recent era of artificial intelligence, LCLU changes are recently being analyzed by supervised and non-parametric machine and deep learning classification algorithms such as Random Forest (RF), Support Vector Machine (SVM), Artificial and deep neural networks (Ge et al., 2020). These are effective and efficient in providing more reliable and accurate results to examine the drivers and impacts on desert or dryland ecosystems (Rash et al., 2023). Among natural factors, droughts are climatically derived extreme events having a significant role in defining the LCLU of dry regions (Costa et al., 2021). Drought indices are derived from measurable hydro-meteorological variables, such as rainfall and temperature. The Standardized Precipitation Index (SPI) is the precipitation-based drought index to accurately define the wetness or dryness of the region (Mckee et al., 1993). Combining meteorological drought indices and LCLU representatives of remote sensing indices like normalized difference vegetation index (NDVI), Normalized difference barren index (NDBaI), and Top grain soil index (TGSI) provides a means to investigate the impacts of extreme events on LCLU in arid regions (Al-Quraishi et al., 2020; Heidari et al., 2023). Previously, Feng et al., (2022a) employed NDVI and TGSI in ML algorithms for desertification monitoring reporting the outperformance of Random Forest algorithm. For instance, a study conducted by E. Damaneh et al. (2019) explored the relationship between droughts and vegetation by correlating the SPI and NDVI in a rangeland ecosystem. A recent study by Gaikwad et al. (2022) also used NDVI as an indicator of LCLU in the region and proved a significant relationship between SPI-based droughts and LCLU change in the region. More recently, de Barros de Sousa et al. (2023) indicated NDVI as a proxy of drought occurrence during SPI detected severe drought events in arid basin of Brazil. Hence, review suggests that LCLU changes in the desert ecosystem are significantly influenced by environmental hazards like meteorological droughts causing land degradation and loss of biodiversity. Addressing and mitigating such impacts could be achieved by adopting low carbon circular economy and active public participation (Chen et al., 2023; Di et al., 2023). A bibliographic review of recent studies encompassing the key words land use, land cover, drought, agricultural drought, SPI, random forest (RF).

Pakistan ranks 5th as climatically vulnerable country in the world with approximately 10 % area covered by desert ecosystems (Ajani and van der Geest, 2021) which majorly comprise rangeland, barren land,

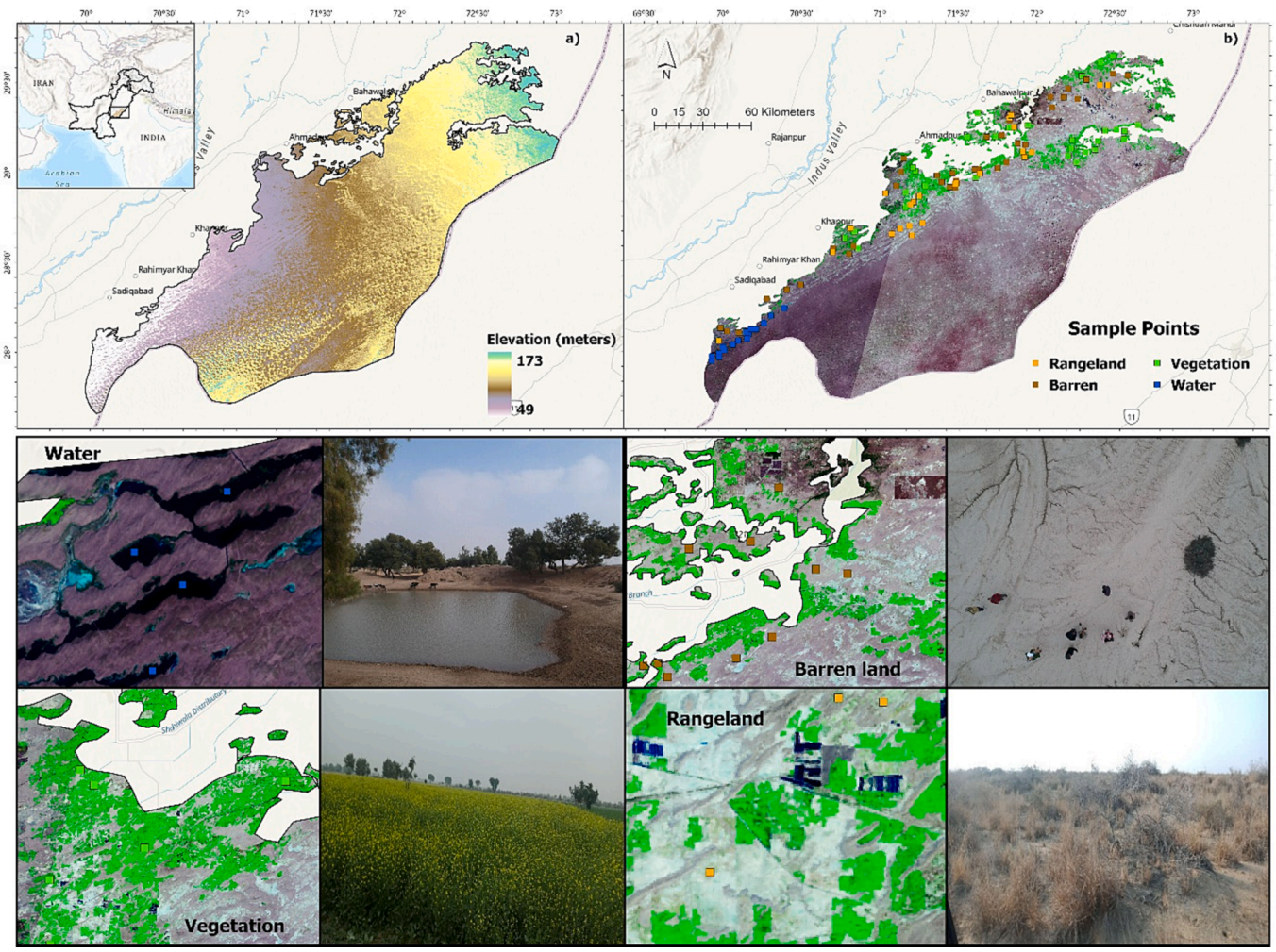

Fig. 2. Location of study area in Pakistan (Cholistan desert), a) Elevation (meters) extracted from USGS/SRTMGL1_003, b) Field samples (water, vegetation, barren, and rangeland) distribution display on Landsat 8 RGB.

and temporary water storage spots (Zubair et al., 2018). Rigorous review of previous studies showed the change detection of LCLU at the district or city level from the context of climate in Pakistan (Arshad et al., 2019; Hussain et al., 2022; Hussain et al., 2019; Majeed et al., 2021; Samie et al., 2020). Change detection of LCLU of desert ecosystem is ignored but substantial to understand the dynamic interactions. Furthermore, meteorological droughts assessments have also remained a keen concern for the researchers in arid zones of Pakistan (Rahman et al., 2021; Ullah et al., 2021). Recent studies regarding the potential impacts of meteorological and agrometeorological droughts in agricultural regions are also reported (Arshad et al., 2023; Bhatti et al., 2023; Ijaz et al., 2023). Nevertheless, examining the dynamics of LCLU of the hyper-arid desert ecosystem in response to climatic change is the identified research gap and still needs to be addressed in Pakistan. Therefore, the research seeks to fill this gap by quantifying LCLU of the desert ecosystem using machine learning based LCLU classification and examining their relationship with meteorological droughts with specific focus on the Cholistan desert. Moreover, this study uniquely explores LCLU dynamics in response to climatic extremes by considering the physical boundary of the desert rather than administrative divisions. In this context, the study surrounds following main objectives; 1) To analyze the LCLU changes from the past three decades in a desert ecosystem employing Random Forest classification and change detection techniques. 2) To examine the SPI-based meteorological droughts (trends and frequency) in the past three decades. 3) To explore the statistical relationship between LCLU changes and meteorological droughts employing linear (Pearson and cross correlation) and non-linear (polynomial regression) approaches (see Fig. 1).

2. Material and method

2.1. Study area

Our study is conducted on a vast deserted region in the southern Punjab of Pakistan called “Cholistan”, between 27°42’−29°45’ North and 69°52’−75°24’ East with an area of 2.6 million hectares (Fig. 2). It is a home to 0.1 million human population with scattered settlement patterns (Akram et al., 2008) and characterized by a harsh climate with scorching temperatures above 50 °C in summer, and less than 0 °C on the colder nights of winter. This desert ecosystem is home to a unique diversity of plants and animal species adapted to survive in the harsh environment (Riaz et al., 2021). Besides, barren, rangeland is the major land cover of the region providing feed to its livestock (Abdullah et al., 2017). Geomorphologically, the region is sub-divided into lesser Cholistan towards the north with irrigated cropland area and greater Cholistan towards the south with more rangeland area. Overall, irrigation improvements have increased the vegetation in northern parts of the region (Akram et al., 2008) but extreme climatic events like droughts have increased the vulnerability of the region towards negative impacts of climatic change in certain years from past decades (Arshad et al., 2022b). Hence, LCLU of the region is majorly dictated by climatic factors like precipitation and temperature which are currently to be addressed

Table 1
Satellite and climate data used in the study.

Satellite data	Dates	Spatial resolution	Product
Landsat 5 TM	8,12,23,13,17,25,28 (Feb-March-1996)	30 M	LCLU, NDVI, NDBaI, TGSI
Landsat 5 TM	14,22,23,10,21,25,28 (Feb-March-2002)	30 M	LCLU, NDVI, NDBaI, TGSI
Landsat 5 TM	22,26,23,15,19,25,26 (Feb-March-2008)	30 M	LCLU, NDVI, NDBaI, TGSI
Landsat 8 OLI	17,12,22,15,17,25,22 (Feb-March-2014)	30 M	LCLU, NDVI, NDBaI, TGSI
Landsat 8 OLI	14,20,13,19,15,27,24 (Feb-March-2020)	30 M	LCLU, NDVI, NDBaI, TGSI
MERRA-2	1990–2020	0.5°×0.625°	Precipitation

Table 2
Land cover/ land use scheme adopted in the study.

Sr. no	LCLU	Description
1.	Barren land	Sandy desert area of the region with sparse herbaceous land cover
2.	Vegetation	Crops grown area of the region or called crop or agriculture land
3.	Rangeland & others	Herbaceous plants and shrubs with mixed desert vegetation
4.	Water	Open or temporary water bodies including open-water reservoirs or ponds (called *Tobas* in local language)

Table 3
Accuracy assessment metrics of RF classification.

Accuracy type	Abb	Formula	Reference
Overall accuracy	OA	$OA = \frac{1}{N}\sum_{i=1}^{r} X_{ii}$	(Fung and LeDrew, 1988; Stehman, 1997)
Producer's accuracy	PA	$PA_i = \frac{X_{ii}}{X_{i+}}$	(Fung and LeDrew, 1988; Stehman, 1997)
User's accuracy	UA	$UA_i = \frac{X_{ii}}{X_{+i}}$	(Fung and LeDrew, 1988; Stehman, 1997)
Kappa Coefficient	K	$K = \frac{N\sum_{i=1}^{r} X_{ii} \sum_{i=1}^{r}(X_{i+} \times X_{+i})}{N^2 - \sum_{i=1}^{r}(X_{i+} \times X_{+i})}$	(Stehman, 1997)
Precision	P	$Precision = \frac{TP}{TP + FP}$	(Rousset et al., 2021; Wardhani et al., 2019)
Recall	R	$Recall = \frac{TP}{TP - FN}$	(Rousset et al., 2021; Wardhani et al., 2019)
F1-score	F1	$F1 = \frac{2 \times Precision \times Recall}{Precision + Recall}$	(Rousset et al., 2021; Wardhani et al., 2019)

in this study.

2.2. Data utilized

Two types of data have been utilized in the study. 1) remote sensing or satellite data products (1990–2020) to examine the LCLU of the region and 2) the meteorological or climatic data (1990–2020) for precipitation to examine and relate the meteorological droughts with the LCLU of the desert ecosystem of the region (Table 1). The detailed description and analytical method of each data are described below.

2.2.1. Remotely sensed data

Satellite data used in the study for LCLU analysis comprises Landsat 5 TM and Landsat 8 OLI to cover the time series from 1990 to 2020. The median image of peak rabi crop season i.e., February-March is selected for the LCLU analysis to achieve high vegetation or agriculture reflection. The study area is covered in 7 distinct path/rows (151/141,150/40,149/39,149/40,150/41,150/39,151/40) on specific dates (Table 1). Time series (1990–2020) of remote sensing indices Normalized Difference vegetation Index (NDVI), Normalized Difference Barren Index (NDBaI), and Top Grain Soil Index (TGSI) are also extracted from the same datasets for the same dates (Table 1). Generally, atmospheric conditions like cloud cover, and satellite sensor calibration might affect the index results. Surface reflectance product of United States Geological Survey USGS, level 2, collection 2 is retrieved in Google-Earth Engine (GEE) for analysis, which is atmospherically corrected, consistent along sensors, radiometrically corrected with improved reflectance values and helped to limit such uncertainties with no initial pre-processing. Moreover, cloud cover was limited to less than 10 % for more accuracy and clear output. Furthermore, field observations for image training also assisted in validating the remote sensing information.

2.2.2. LCLU classification scheme

Based on the extensive field observations and ground truthing of the region, the following classification scheme is developed to address the LCLU of our study area (Table 2).

2.2.3. Random forest classification

The GEE is a powerful cloud computing online platform that provides an opportunity for various machine learning classification algorithms (Shafi et al., 2023) including decision trees (DT), smile Cart, Support Vector Machine (SVM), Random Forest (RF), etc. to perform land cover/ land use classification. Currently, we adopted the widely used RF classifier of LCLU analysis of the region for the specific years of 1996, 2002, 2008, 2014, and 2020.

Random Forest is an ensemble, non-parametric machine learning method which excel to solve both classification and regression or prediction problems. The algorithm works by creating an ensemble of decision trees, each of which is trained on a different subset of the input data. These decision trees are created using bootstrap sampling, where each subset is created by randomly selecting data instances from the input data set with replacement (Mateen et al., 2023). At each node of decision tree, a random subset of features is considered for splitting, enhancing the generalization of model. During training stage, each decision tree uses a random subset of the available features to make its splits, which helps to reduce the correlation between the trees and improve the accuracy of the final predictions. Once the decision trees are trained, they can be used to classify new data by computing the class probabilities for each tree and then averaging the results across all the trees. Hence, combination of random feature selection and diverse trees facilitates to mitigate the overfitting making the model resilient to noise. Furthermore, feature importance allows the users to assess the contribution of each extracted feature for accurate predictions. In Google-Earth Engine, the ee.Classifier.randomForest method is used to implement the random forest algorithm, allowing users to classify large-scale remote sensing data with high accuracy and efficiency (Ge et al., 2020).

Labelled training samples from each LCLU were collected through GPS/drone-based ground truth field observations between 2019 and 2020. Number of field points were collected randomly according to LCLU proportion and accessibility to reach (Fig. 2). Remote areas of the desert and images of previous years were interpreted and trained from high resolution imageries of Google Earth Pro, and visual interpretation techniques. Finally, all field samples were collected in ArcGIS pro and uploaded in the assets of GEE as training input. Finally, around 5000 to 7000 reference points are generated on the whole study area in different years combining field observations and manual image training in GEE. Afterwards, these were randomly set to 80 % for training and 20 % for testing or validation to verify the accuracy of RF classification as also proposed by Feng et al., (2022b). The significant arguments of parameters suggested in the RF classifier in GEE include the number of trees (ntrees) which may range to 100 – 500 or more and currently based on different classification trials is set to 350, variables per split (mtry) which is currently set to 5 (if unspecified uses the square root of the variables classified).

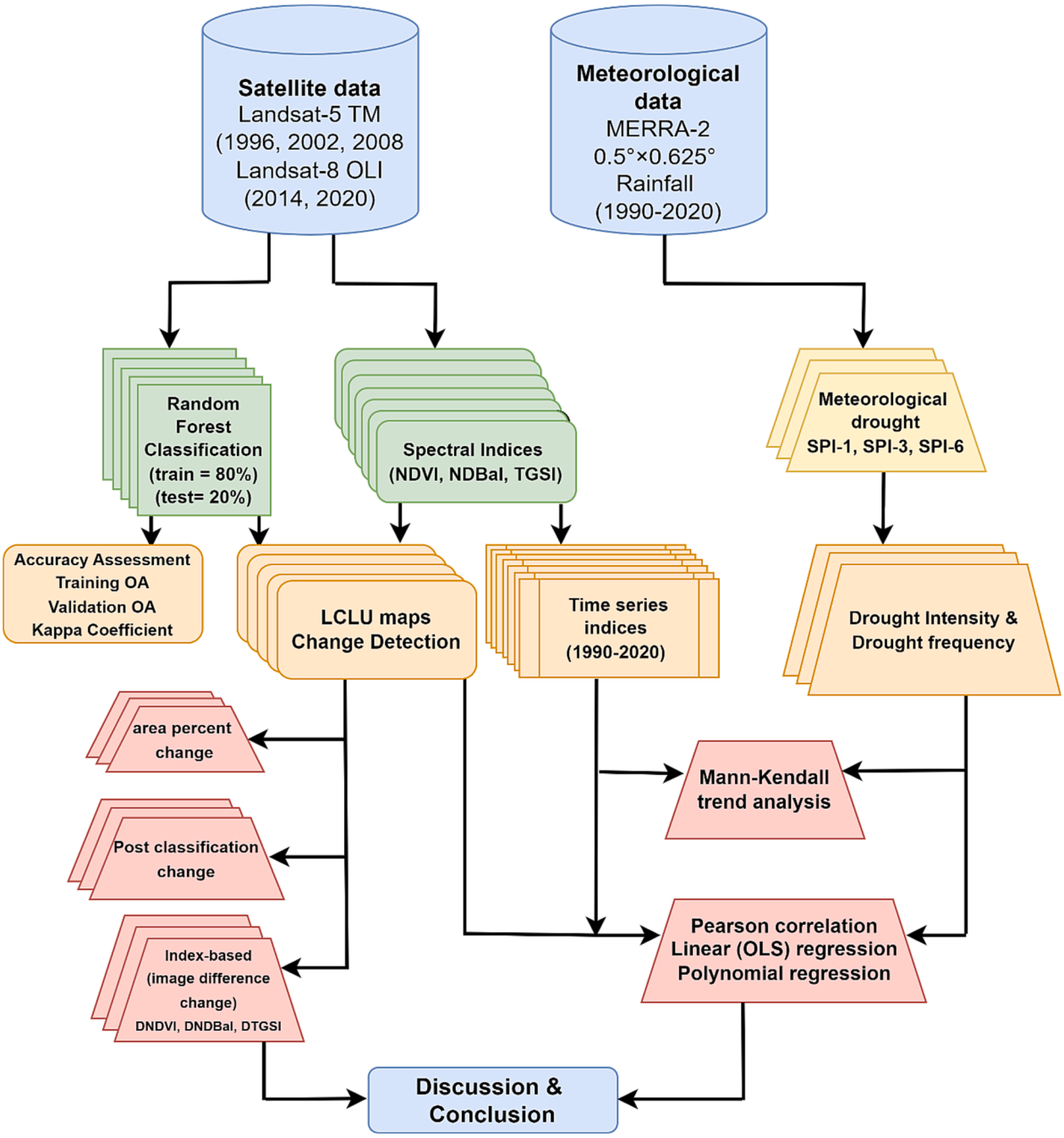

Fig. 3. Methodological framework of the study.

2.2.4. Accuracy assessment

After LCLU classification, a confusion matrix and validation matrix is generated computing producer's and user's accuracy, Overall accuracy (OA) and Kappa Coefficient (K) (Table 3) to assess the performance of ML classification (Chughtai et al., 2021).

Where OA is the overall accuracy, PA_i is producer accuracy and UA_i is the user accuracy and Kappa Coefficient K is presented in Table 3. Where N presents the total number of observations, r presents the rows and columns (numbers) in the error matrix, X_{ii} presents the number of observations in columns and rows i (the diagonal element), X_{i+} and X_{+i} are the marginal totals of columns and rows (Mawenda et al., 2020; Tariq et al., 2022). Overall accuracy and kappa statistics are the most significant metrics used to evaluate the accuracy of land cover classification. The kappa value of less than or equal to 0.4 indicates poor agreement between classified variables, k = 0.4 – 0.8 presents moderate to strong agreement, and above 0.8 presents very strong agreement between classified variables (Mawenda et al., 2020). F1-score is also used to evaluate the RF model performance, calculated following the precision and recall computation from the confusion matrix following the equation (5) to 7). Precision measures the accuracy of the model when it predicts positive outcomes, indicating how many of these predictions are correct. Recall measures the proportion of true positive instances that were successfully retrieved by the model, providing insight into how well the model captures the complete set of actual positive instances (Alem and Kumar, 2022). TP is the true positive, FP is the false positive, and FN is the false negative. The harmonic mean of precision and recall defines the F1-score and ranges between 1 (high precision and recall) and 0 (lowest precision and recall) and measured the robustness of RF classification (Alem and Kumar, 2022; Waleed et al., 2023).

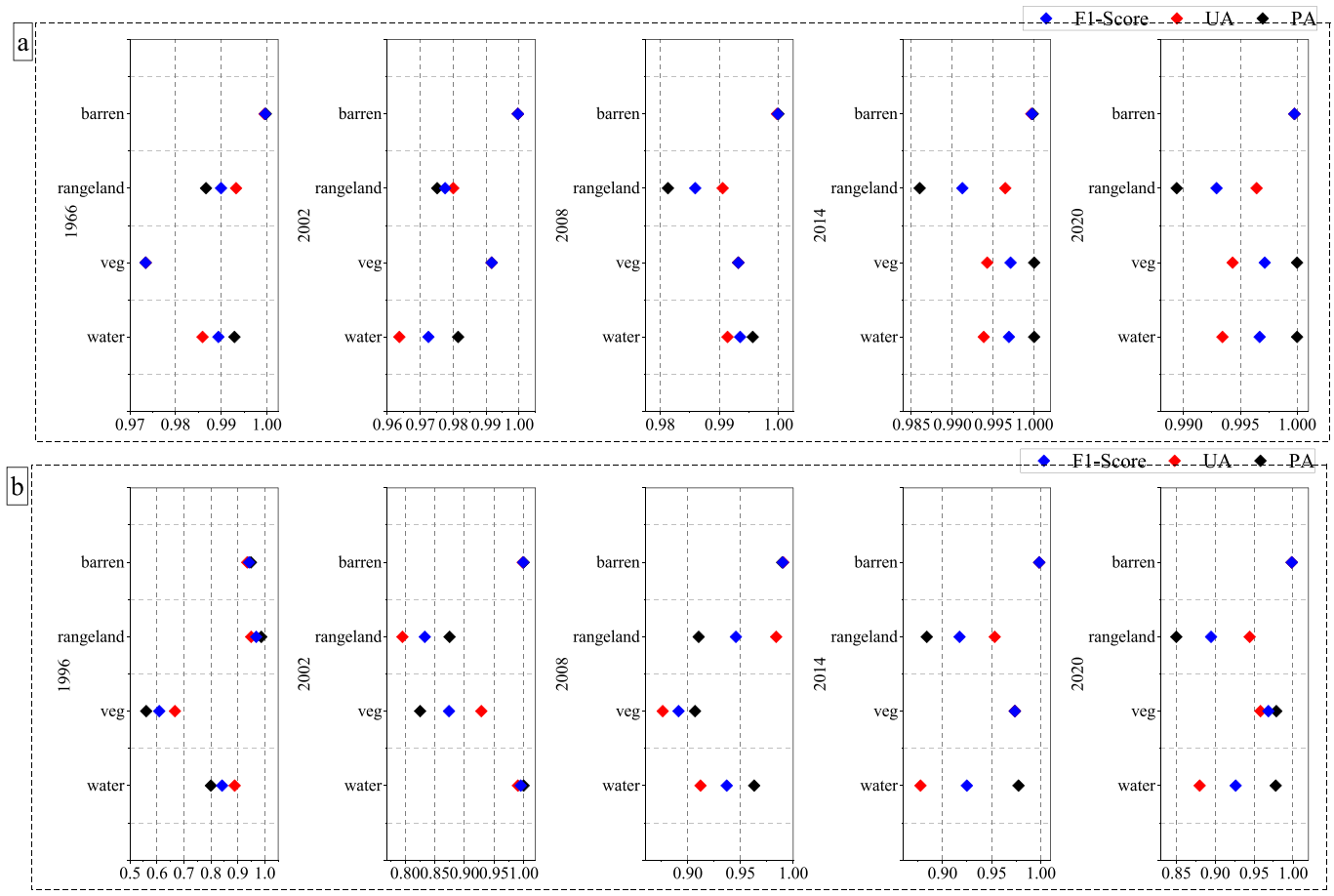

Fig. 4. Accuracy assessment of individual LCLU from confusion and validation metrics of RF classification (PA, UA, F1).

Table 4
Overall accuracy and Kappa coefficient for RF classification in respective years of LCLU classifications.

Years	T (OA)	T (kappa)	V (OA)	V(kappa)
1996	0.99	0.99	0.80	0.69
2002	0.99	0.99	0.98	0.96
2008	0.99	0.99	0.99	0.99
2014	0.99	0.99	0.99	0.96
2020	0.99	0.99	0.99	0.96

T (OA) = Training Overall Accuracy, V (OA) = Validation Overall Accuracy.

2.2.5. *Change detection of LCLU classification*

After performing land cover/land use classification for representative years, three different methods of change detections are employed to examine the area and percent change from one class to another which are described as.

2.2.5.1. Area/percent change detection. Area and Percent change or rate of change is the widely applied quantitative LCLU change detection methods revealing the magnitude of loss and gain of each land cover/land use in the region (Opedes et al., 2022) currently in hectares and percentage %. Mathematically, it is presented through following equations (3) and 4):

$$Change\ areaCA_{ha} = LCLU_{i+1} - LCLU_i \quad (1)$$

$$\%Change\ areaCA_{ha} = \%LCLU_{i+1} - \%LCLU_i \quad (2)$$

Where $LCLU_i$ is the land cover/land use area of a particular class in the previous year i and $LCLU_{i+1}$ presents the land cover/land use area of a particular class in the recent year $i+1$. All classified images were imported into ArcGIS pro from GEE for area computation, post classification and index based change detection analysis.

2.2.5.2. Post classification or categorical change detection. Post classification change detection (PCCD) is another powerful technique to quantify and identify the landcover/land use conversions based on the principle of "FROM-TO" change analysis between all land use categories (Thakkar et al., 2017). The results of post classification change detection are highly dependent on LCLU classification and provide meaningful quantitative and qualitative results (Chughtai et al., 2021; Peiman, 2011). The qualitative results of PCCD are presented in the form of categorical change maps in the respective years (1996–2002, 2002–2008, 2008–2014, 2014–2020) while quantitative results are presented in the form of cross-tabulation matrix presenting the area change from one class to another in all respective years.

2.2.5.3. Index based change detection (IBCD). Index based change detection in another quantitative and qualitative change detection method (Sarp and Ozcelik, 2017) employs significant land use indices which leads to "Difference image" analysis (Arshad et al., 2022a; Ridd and Liu, 1998). Based on LCLU characteristics of the region, currently, three indices are employed as a representative of major land cover for IBCD. These include:

***Normalized difference vegetation index (NDVI)*:** measures the normalized difference ratio between near Infrared (NIR) and red band (RED) of satellite data. NDVI ranges between −1 (no vegetation) to + 1 (healthy vegetation) (Tucker, 1979). Water is mostly reflected in the red band and gains a negative NDVI value while barren / built surfaces gain a value near 0, while positive values reveal the presence of vegetation.

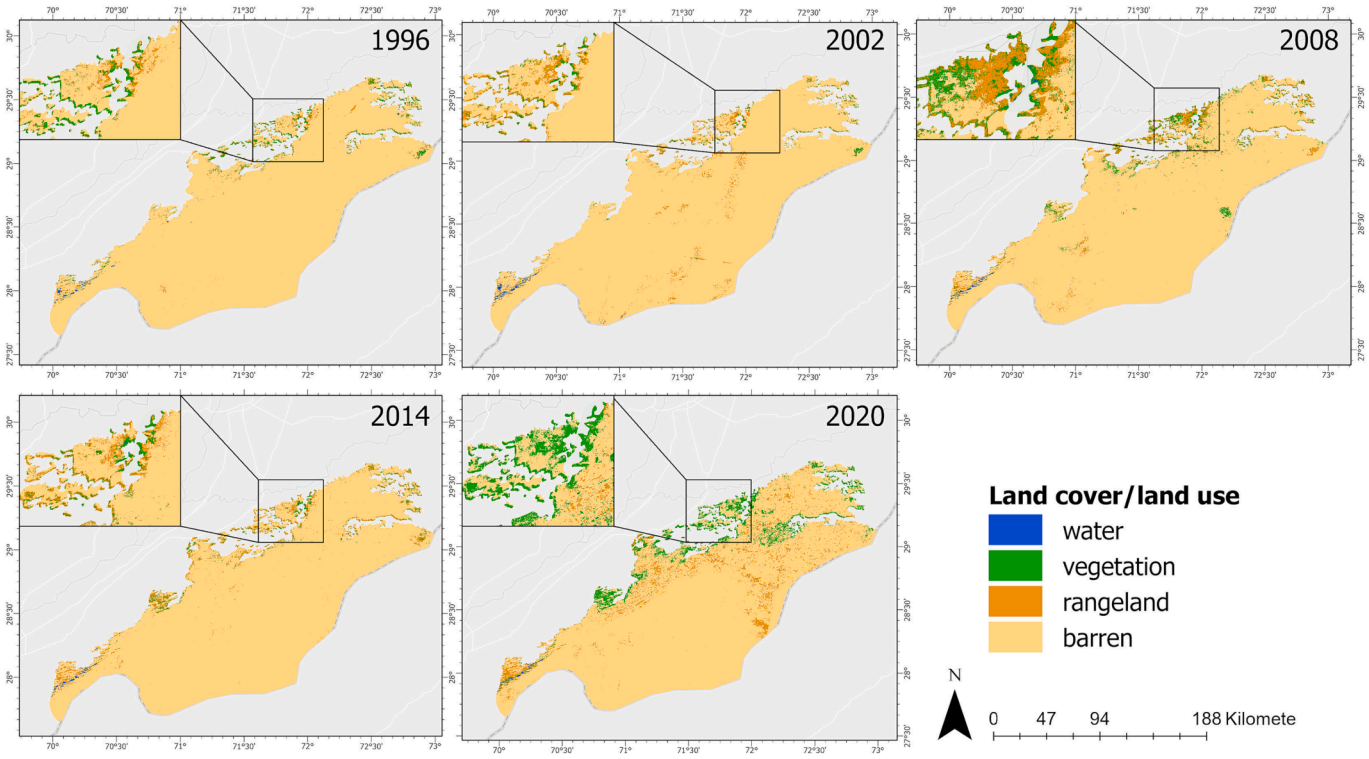

Fig. 5. Land cover/land use pattern derived from supervised (Random Forest) classification.

Table 5
Area (hectares) and percent occupied by each LCLU in respective years.

Land use Categories	1996		2002		2008		2014		2020	
	Area (ha)	(%)	Area (ha)	(%)	Area (ha)	(%)	Area (ha)	(%)	Area (ha)	(%)
Water	5,015	0.1	7,085	0.15	4,435	0	4,525	0	3,096	0.1
Vegetation	47,617	2	22,644	0.8	67,830	2	33,444	1	160,570	5.4
Range Land & Other	43,774	1	77,917	2.6	107,288	4	106,679	4	170,158	5.7
Barren Land	28,74,308	97	28,63,068	96	27,91,162	94	28,26,066	95	26,36,890	88.7

Currently, NDVI represents the vegetation land use of the region.

$$NDVI = \frac{NIR - RED}{NIR + RED} \tag{3}$$

Normalized difference barren index (NDBaI): measures the normalized difference ratio between short wave infrared (SWIR) and thermal infrared (TIR) of satellite data. The value of NDBaI also ranges between −1 (water and vegetation) to + 1 (Barren surfaces) (Arshad et al., 2022a; Moisa et al., 2022). Currently, NDBaI is employed as representative of Barren land of the region.

$$NDBaI = \frac{SWIR - TIR}{SWIR + TIR} \tag{4}$$

Top grain soil index (TGSI): TGSI is widely applied index in barren and desertification studies and presents the spectral reflectance properties (texture and size) of sandy soil in desert ecosystems with a good correlation with field observed sand size of topsoil (Xiao et al., 2006).

$$TGSI = \frac{RED - BLUE}{RED + GREN + BLUE} \tag{5}$$

Where red, green, and blue indicate the reflectance of the Landsat TM and OLI sensors in bands. The TGSI also ranges from −1 (vegetation and water bodies) to + 1 (sandy soil). The sand content increases with increasing positive value revealing a good deal of desertification in the region (Mihi et al., 2022).

After deriving image indices, difference image indices by subtracting the recent year index from the previous or initial year image index and are better presented by the following equations.

$$DNDVI = NDVI_{2020} - NDVI_{1996} \tag{6}$$

Where *DNDVI* presents the difference image of NDVI, $NDVI_{2020}$ is the NDVI image for the year 2020 and $NDVI_{1996}$ is the NDVI image of the year 1996.

$$DNDBaI = NDBaI_{2020} - NDBaI_{1996} \tag{7}$$

Where *DNDBaI* presents the difference image of NDBaI, $NDBaI_{2020}$ is the NDBaI image for the year 2020 and $NDBaI_{1996}$ is the NDBaI image of the year 1996.

$$DTGSI = TGSI_{2020} - TGSI_{1996} \tag{8}$$

Where *TGSI* presents the difference image of NDVI, $TGSI_{2020}$ is the TGSI image for the year 2020 and $TGSI_{1996}$ is the TGSI image of the year 1996. The values of difference image index vary from −1 (presenting loss or decrease), 0 (presenting no change), +1 (presenting a gain or increase). Hence, the gain and loss of one index is often compensated by the gain and loss of another index which reveals the change of a particular LCLU (Arshad et al., 2022a; Chen et al., 2020).

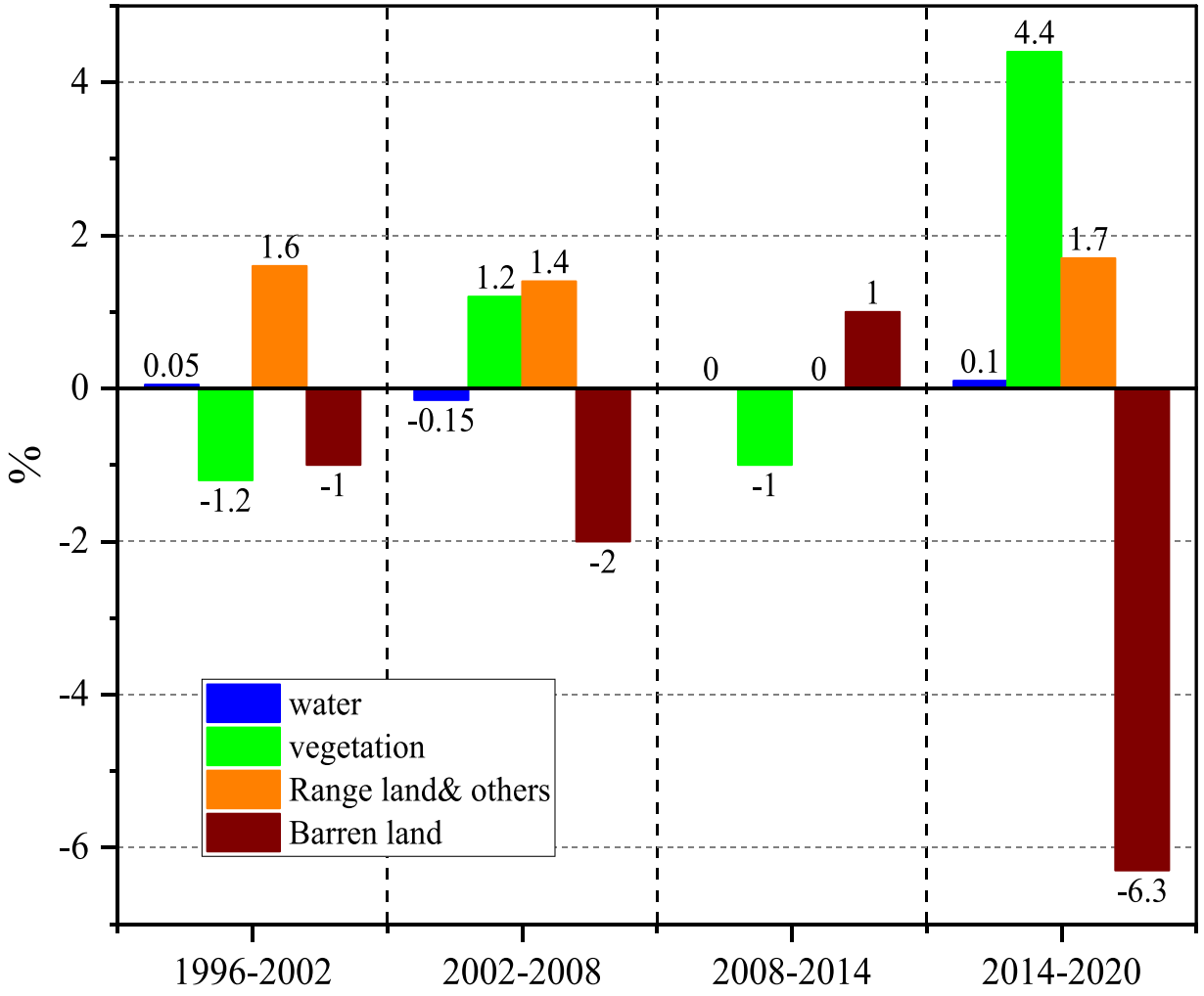

Fig. 6. Area based change detection of LCLU in respective time periods.

Table 6
Area/percent change in LCLU in respective time periods.

Land use	1996–2002		2002–2008		2008–2014		2014–2020	
	Change area (ha)	% change	Change area (ha)	% change	Change area (ha)	% change	Change area (ha)	% change
Water	2,070	0.05	−2,650	−0.15	90	0	−1,429	0.1
vegetation	−24,973	−1.2	45,186	1.2	−34,386	−1%	127,126	4.4
Range land & others	34,143	1.6	29,371	1.4	−609	0	63,479	1.7
Barren land	−11,240	−1%	−71,906	−2	34,904	1 %	−189,176	−6.3

2.2.6. Meteorological drought analysis

Due to the absence of a meteorological station in the desert, single point meteorological or climatic data used for drought analysis i.e., rainfall (R) is derived from satellite-based reanalysis product of NASA, Modern-Era Retrospective analysis for Research and Applications (MERRA-2) version 2 with a 0.5° × 0.625° gridded spatial resolution (Gelaro et al., 2017). The central single point (centroid) of the desert is considered as a representative of whole region and the data is acquired from 1990 to 2020 for unified three decadal LCLU and droughts analysis. The reanalysis product is consistent and validated for use in several climatic and extreme events studies in arid and other regions (Arshad et al., 2021; Ullah et al., 2021). For instance, the validity of MERRA-2 climatic product is proven with the R^2 of 0.9 in the same region (Arshad et al., 2022b).

The climatic conditions of the region are quite vulnerable to extreme events like droughts; therefore, the meteorological characteristics of the region are examined in relation to LCLU change in the district. The standardized precipitation index (SPI) is a widely accepted meteorological drought index to analyze the influence of precipitation characteristics in varied temporal scales (Mckee et al., 1993). The SPI usually measures the short term from 1-month (SPI-1) to long term e.g., 36-months (SPI-36) drought conditions of the region. For instance, currently, SPI-1, SPI-3, and SPI-6 are computed to examine the short to medium range drought conditions from 1990 to 2020 in relation with LCLU in the desert region of Pakistan. Currently, we computed the SPI using "SPEI" package in R environment using gamma density distribution $G(x)$.

Table 7
Post classification (categorical change) in respective time periods.

	2020			
1996	**water**	**Vegetation**	**Rangeland**	**Barren**
Water	–	474	1,731	212
Vegetation	173	–	2,514	6,106
Range land	217	26,224	–	11,599
Barren	110	95,047	160,179	–
	2002			
1996	**water**	**Vegetation**	**Rangeland**	**Barren**
Water	–	57	419	949
Vegetation	600	–	20,930	12,120
Range land	150	5,207	–	20,477
Barren	174	3,415	39,628	–
	2008			
2002	**water**	**Vegetation**	**Rangeland**	**Barren**
Water	–	633	1,685	1,040
Vegetation	373	–	12,130	1,054
Range land	183	11,698	–	31,177
Barren	157	46,413	58,614	–
	2014			
2008	**water**	**Vegetation**	**Rangeland**	**Barren**
Water	–	468	553	74
Vegetation	238	–	21,420	32,363
Range land	756	11,522	–	38,189
Barren	193	7,644	27,884	–
	2020			
2014	**water**	**Vegetation**	**Rangeland**	**Barren**
Water	–	816	639	82
Vegetation	22	–	828	4,250
Range land	86	68,204	–	22,240
Barren	0.36	63,206	152,542	–

$$G(x) = \frac{1}{\beta\Gamma(\alpha)} x^{\propto -1} e^{-x/\beta}, x > \tag{9}$$

$$SPI = \frac{xi - \overline{x}}{\sigma} \tag{10}$$

Where $\Gamma(\alpha)$ is the gamma function, α is the shape and β is the scale parameter. $x > 0$ is the precipitation parameter (Lloyd-Hughes and Saunders, 2002). And xi is the precipitation of a particular month, $\overline{x}$ is the long term mean of precipitation and σ is the standard deviation (Salvacion, 2021). The negative or below 0 values of SPI presents the dry or drought while positive or above 0 values present the wet conditions of the region. After the identification of drought years in the time series, yearly drought frequency (in months) is calculated using the formula:

$$DF = \frac{D_{months}}{N_{months}} \tag{11}$$

Where D_{months} presents the number of months in one year with drought conditions and N_{months} is the total number of months in one year (i.e., 12).

2.2.7. Temporal (time series) analysis of LCLU changes and meteorological droughts

Our study aimed to examine the changes in LCLU of the desert region in response to meteorological drought characteristics over the past 3 decades. Time series of the selected indices (NDVI, NDBaI, and TGSI) are extracted from GEE from 1990 to 2020 from Landsat satellite data to explore its relationship with the time series of SPI-drought. Hence, to examine the variable's trend and relationship, we employed the Mann-Kendall test, Pearson correlation, linear and polynomial regression. The complete methodological framework of the study is presented in Fig. 3.

2.2.7.1. Mann-Kendall (MK) trend test and Sens's slope (Ss). Mann-Kendall is one the widely used non-parametric trend test to examine the long-term monotonic trend in the time series (Mann, 1945). The MK test is an applied trend test in various climatology and hydrology studies (Liu et al., 2016). It assumes of Null hypothesis which states that "there is no significant trend existing in the time series" versus an alternate hypothesis stating that "there is a significant trend in the time series" (Kendall, 1948). The MK test results provide the Kendall (Tau) value, p-value (at 95 % confidence), and z-statistics. The positive z-score reveals the increasing and the negative value of z-score reveals the decreasing trend of the variable in the time series. To determine the slope or direction of change, Sens's slope is employed, with a positive value presenting the increasing trend of a variable and a negative value revealing the decreasing trend of the variable (Sen, 1968). Hence, MK test and Sens's slope are employed to the long-term time series (1990–2020) of remote sensing indices (NDVI, NDBaI, and TGSI) extracted from the online cloud computing platform of GEE and meteorological drought indices (SPI-1, SPI-3, and SPI-6).

2.2.7.2. Linear and non-linear regression fit between LCLU and drought indices. Furthermore, to examine the linear and non-linear relationship between LCLU variables and meteorological droughts Pearson correlation R and coefficient of determination R^2 is employed at the significance of ($p < 0.05$, $p < 0.01$, $p < 0.001$). Pearson correlation is presented by the equation:

$$r = \frac{\sum(x_i - \overline{x})(y_i - \overline{y})}{\sqrt{\sum (x_i - \overline{x})^2 \sum \ (y_i - \overline{y})^2}} \tag{12}$$

Where x_i and y_i are the variables and $\overline{x}$ and $\overline{y}$ are the mean of variables. Moreover, to elaborate the potential time lag between drought events and subsequent land use change, cross correlation is applied. Cross correlation is an advanced statistical method used to measure or quantify the similarity between two signals (values) by comparing their respective time shifts in a time series. It measures the correlation between two datasets at different time lags to in-depth understand the temporal relationships (Yamaki et al., 2021). Currently, SPI-1, SPI-3, and SPI-6 are cross correlated with major LCLU representatives of the region i.e., NDVI, NDBaI, and TGSI.

Coefficient of determination R^2 is determined by the linear and non-linear (polynomial) fitting of the variables.

$$R^{2=}1 - \frac{RSS}{TSS} \tag{13}$$

Nine individual linear and polynomial regression models are fitted to determine the high value of R^2 to reveal the best form of relationship between the variables. The individual models are fitted between (NDVI vs SPI-1, SPI-3, and SPI-6, NDBaI vs SPI-1, SPI-3, and SPI-6, and TGSI vs SPI-1, SPI-3, and SPI-6). In our models, remote sensing indices (NDVI, NDBaI and TGSI) are used as a separate dependent variable (Y) to be predicted from meteorological droughts X (SPI-1, SPI-3, and SPI-6).

Linear regression is a widely applied supervised statistical learning approach to determine the linear relationship in vegetation studies (Bera et al., 2021; Li et al., 2019; Roy, 2021). It provides an accurate prediction with a high value of R^2. Mathematically, it is presented as

$$Y_{exp} = \beta_{\circ} + \beta X \tag{14}$$

However, to explore the non-linear relationship between the variables, a 3rd order polynomial fit is applied. Mathematically, a polynomial fit is presented by the following equation:

$$Y_{exp} = \beta_{\circ} + \beta_1 X + \beta_2 X^2 + \beta_3 X^3 + \cdots \beta_n X^k + \epsilon \tag{15}$$

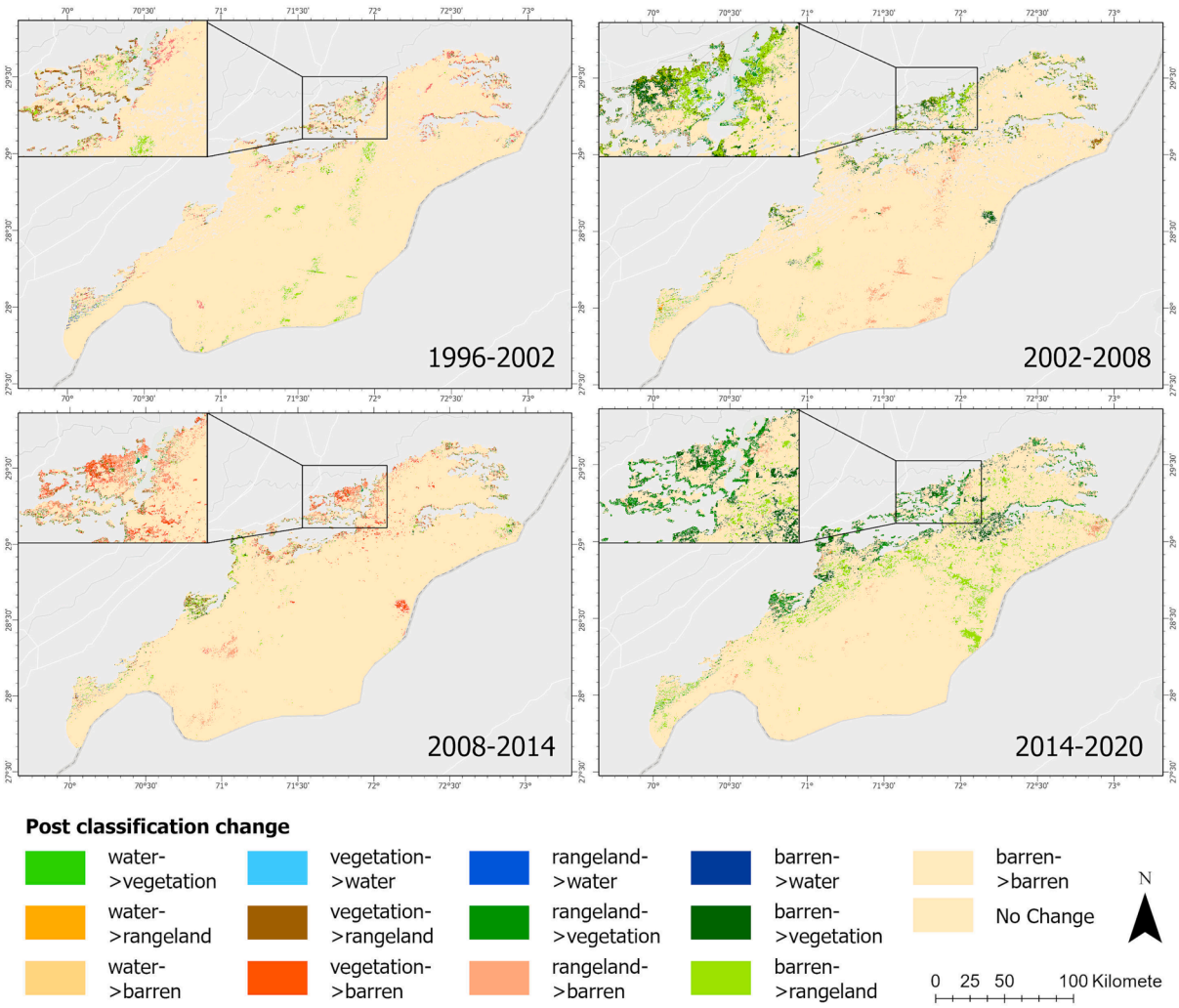

Fig. 7. Spatial pattern of categorical change ("From > To") in all respective years.

Where Y_{exp} presents the expected predicted variable, $\beta_{\circ}$ presents the intercept and β_1, β_2, and β_3 are the X coefficients or predictors of Y. K presents the degree of the polynomial (currently it is 3) and ϵ is the residual (Bera et al., 2021; Bradley and Srivastava, 1979; Gertner et al., 2002).

3. Results

3.1. Landcover/land use characteristics of Cholistan region

Results of the accuracy assessment from RF classifier revealed the highest PA, UA, and F1-score of 0.999 for barren in all years. The vegetation accuracy in 1996 was 0.973 for PA, UA, and F1 which improved to 1 and 0.999 for PA, UA, and F1-score in 2020 (Fig. 4). Furthermore, overall validation accuracy was improved from 80 % in 1996 to 99 % in the years 2020 presented in Table 4. Kappa coefficient of the validation set is also found to be in high satisfaction i.e., 0.69 in 1996, and 0.96 in 2002, 2014, and 2020 followed by 0.99 in 2008 (Table 4).

Results derived from supervised classification reveal that water resources in the Cholistan desert contributed 5,015, 7,085, 4,435, 4,525 and 3,096 ha of the total land area in the respective years of 1996, 2002, 2008, 2014 and 2020 with a proportion 0.1 %. The vegetation area of the desert accounted for 47,617 ha in 1996 which decreased to 22,644 ha in the year 2002 making 0.8 % and again raised to 2 % in 2008 with 67,830 ha of total land area (Fig. 5). In the year 2014, half of the vegetation land area decreased with a contribution of 33,444 ha of total land area and significantly raised to 160,570 with 5.4 % of the total. Likewise, the rangeland area of the region increased from 43,774 ha in 1996 to 77,917 ha in 2002, 107288 ha in 2008, 106,679 ha in 2014 and 170,158 ha in 2020 with a proportionate increase from 1 % to 5.7 % in time span of 24 years (Table 5). The largest proportion i.e., about 97 % of LCLU of the desert is barren land with 28,74,308 ha in the year 1996 which decreased to 11,240 ha making 96 % in 2002. Furthermore, it also reduced to 27,91,162 ha in the year 2008 and 28,26,066 ha in 2014. Barren land area of the desert drastically decreased to 26,36,890 ha with a proportion of 88.7 % in 2020 at the expense of vegetation and rangeland increase (Fig. 5, Table 5).

3.2. Change detection of land cover/ land use in Cholistan region

Change detection of land cover/land use in the region is observed by the following methods.

3.2.1. Area/percent change

Land cover/ land use change detection revealed a minor gain of 2,070 ha (0.05 %) in water resources of the desert followed by a significant loss of −24,973 ha (-1.2 %) in vegetation or agricultural land, and 34,143 ha (1.6 %) gain in range land and reduction of −11,240 ha (-1%) barren land from 1996 to 2002. The next time span of 2002–2008 revealed a minor reduction of −2,650 ha (-0.15 %) in water resources of the region and 45,186 ha (1.2 %) gain in vegetation followed by 1.4 %

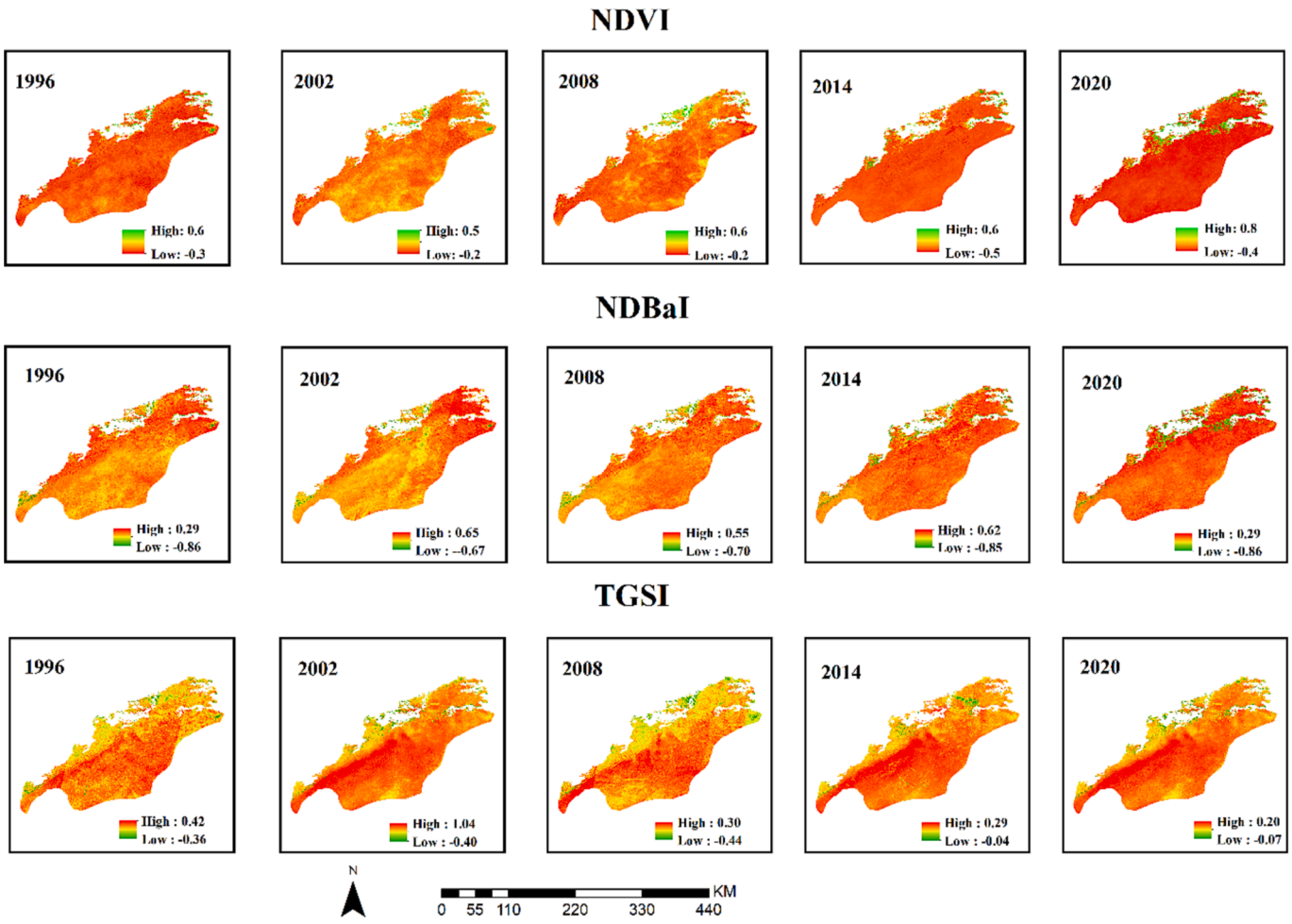

Fig. 8. Time series of remote sensing indices in respective years of LCLU classifications.

gain in range land of the region. The gain in vegetation (agricultural & rangeland) resources of the region took place at the expense of −71,906 ha (-2%) reduction in a barren land of the region. Afterward, vegetation resources of the region decreased by −1% at the expense of 1 % gain in barren land of the region (Fig. 6, Table 6). The last time span of 2014–2020 experienced the most significant changes in land cover/land use of the region where vegetation or agricultural land experienced a net gain of 127,126 ha (4.4 %) followed by 63 479 ha (1.7 %) by range land. This significant gain in land use in this period occurred at the expense of −189,176 ha (-6.3 %) reduction of barren land in the region (Fig. 6, Table 6).

3.2.2. *Post classification (categorical) change detection*

Land use transfer matrix derived from categorical post classification change detection presents the variation of interconversions of different land use types in all time spans. Overall. the most significant interconversions from 1996 to 2020 occurred between barren, vegetation, and rangeland. The highest conversion of 160,179 ha occurred from barren to rangeland area followed by 95,047 ha of barren to vegetation and 26,224 ha from rangeland to vegetation. However, the 1st time span from 1996 to 2002 also revealed the largest conversion of 39,628 ha from barren to rangeland followed by 20,930 ha conversion of vegetation to rangeland. Apart from the barren to rangeland conversion, 20,477 ha of rangeland from greater Cholistan also degraded into barren land followed by 12,120 ha of degradation of vegetation to barren land. Transformation of barren to vegetation is observed to be very low i.e., 3,415 ha. Thus, the 1st time span of LULC change reveals more degradation of vegetation land use. The next time span from 2002 to 2008 reveals a 58,614 ha conversion of barren to range land followed by 46,413 ha conversion of barren to vegetation. Other than these, 31,177 ha of rangeland also converted into barren land in some parts of the desert while 11,698 ha of rangeland land also converted into vegetation significantly from lesser Cholistan, i.e., towards the northern belt of the region (Table 7, Fig. 7). Hence, this time span reveals more conversions towards rangeland and vegetation with less land degradation. Furthermore, the next time span from 2008 to 2014 revealed the highest rangeland and vegetation degradation i.e., 38,189 ha of rangeland to barren land conversion followed by 32,363 ha of vegetation to barren land conversion. On the other hand, 27,884 ha of barren land also converted into new rangeland and 11,522 ha and 7,644 ha conversion of rangeland and barren land to vegetation respectively. The last time span from 2014 to 2020 resulted the highest gain with 152,542 ha and 63,206 ha conversion of barren to rangeland and vegetation respectively. Moreover, 68,204 ha rangeland also converted into vegetation. Overall, the total vegetation gain in this time span is found to be 132,226 ha from all land use conversions which is the highest that all early time spans (Table 7, Fig. 7).

3.2.3. *Index based change detection*

Another significant change detection technique applied currently is index-based change detection employing NDVI, NDBaI and TGSI (Fig. 8). Descriptive statistics of applied indices revealed an increase of maximum NDVI 0.67 in 1996 to 0.89 in 2020 with a standard deviation of 0.02 to 0.12. Contrary, the maximum, and mean NDBaI of the region was 0.29 and 0.10 in 1996, increased in 2002–2014 and rapidly fall to a maximum 0.29 again in 2020 which is attributed to an increase in NDVI.

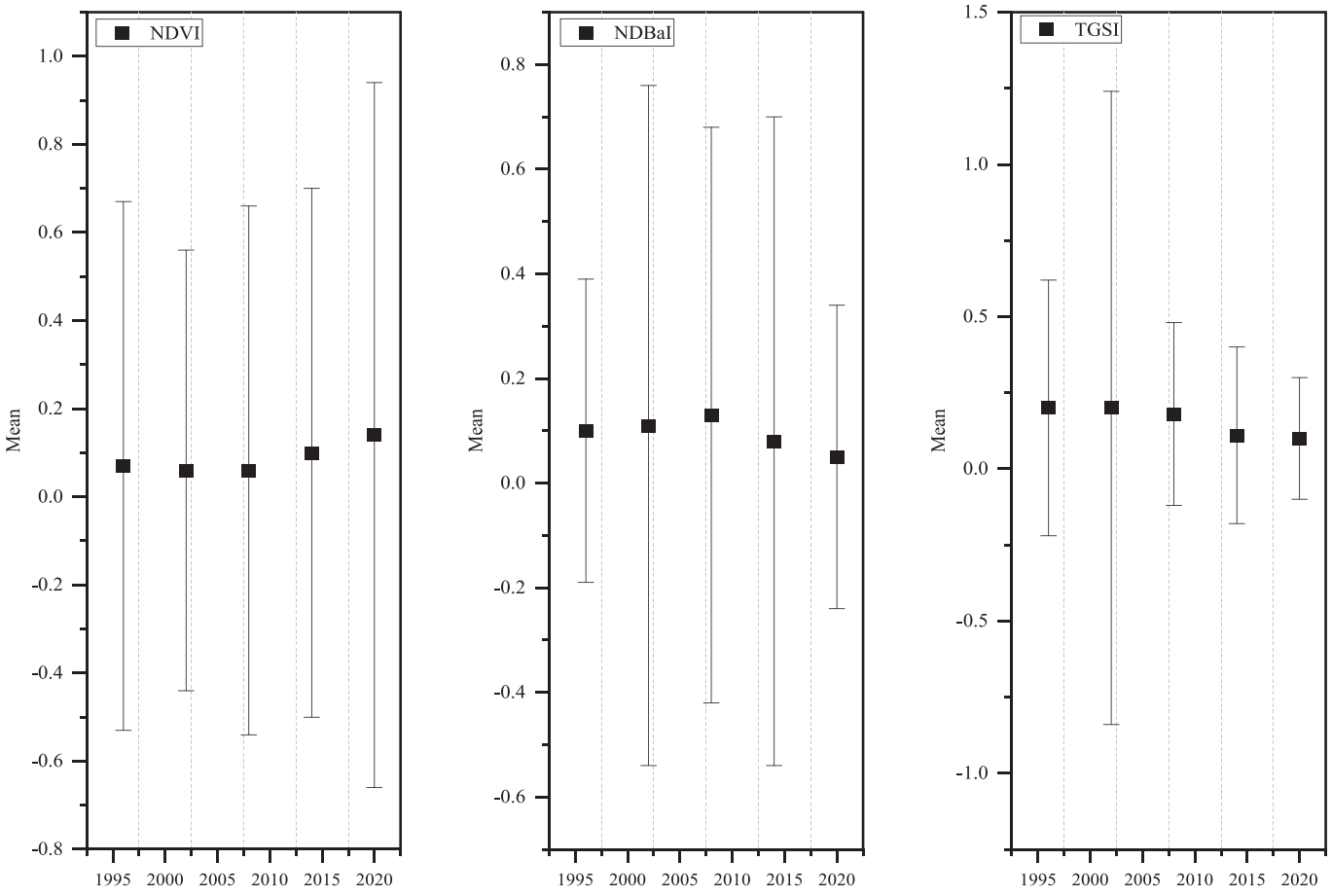

Fig. 9. Descriptive (min, max and mean) analysis of NDVI, NDBaI, and TGSI in respective time series.

TGSI observed a decline from 0.42 in 1996 to 0.20 in 2020 (Fig. 9). Index change computation revealed a good dynamic between all indices (Fig. 10). NDVI change (1996–2020) revealed a high increase of 3.76 % followed by a 2.66 % low increase. On the contrary 48 % low decrease is also observed with 44 % no change (Table 8 and Fig. 9). Like other change detection methods, index-based change analysis also revealed that the high increase of NDVI took place at the expense of 2.72 % high and 3.34 % low decrease in NDBaI of the region. Similarly, TGSI also experienced a 1.5 % high and 6 % low decrease compensated by NDVI increase. Hence, the index-based change detection verifies the classified based change detection methods presenting a good deal of inverse relationship between vegetation and Barrenness of the region which is further explored by climatic conditions of the region in the next section.

3.3. Meteorological droughts (SPI) characteristics of the Cholistan region

To examine the influence of climatic characteristics of the region on LCLU changes in the region, meteorological drought analysis revealed that the region remained quite vulnerable towards short term to long term drought conditions here. SPI-1, SPI-3, and SPI-6 revealed several dry and wet years in the past three decades (Fig. 11a). In the 1st decade of 1990 s, 4 drought years (1990, 1991, 1998, and 1999) are identified as dry years with low to high droughts. The 2nd decade of 2000 s revealed a longer drought spell from 2000 to 2005 based on SPI-1 while the year 2005 is not identified as dry or drought year by SPI-3 and SPI-6. The 3rd decade experienced fewer drought years as compared to the past. SPI-1 revealed only two (2018, 2019) as drought years followed by three (2014, 2018, and 2019) drought years as identified by SPI-3 and SPI-6 (Fig. 11a). Yearly droughts frequency (in months) presented in Fig. 11b revealed a rise of 1-month (SPI-1) drought frequency in the region. 90 % of drought months are observed in the recent past of the year 2018 followed by 75 % of drought months in the year 2000 and 50–66 % of drought months in the years 1990 and 2002. Drought frequency analysis of SPI-3 revealed the years 2000 with 100 % drought frequency followed by 91 % in 1991 and 83 % in year 2002 and 2018. SPI-6 analysis revealed 1991, 2002 and 2004 with 100 % drought frequency followed by 90 % drought frequency in 2018.

3.4. Temporal analysis of land cover / land use and meteorological droughts

To examine the influence of meteorological droughts on LCLU characteristics and changes in this arid ecosystem of Cholistan, the results of three types of tests or analysis (Trend analysis, Pearson correlation, and linear and non-linear regression) are presented below.

3.4.1. Trend (Mann-Kendall and Sen's slope) analysis of all variables

Mann-Kendall's trend test along with Sen's slope of applied remote sensing and meteorological droughts indices on a time-series of 3 decades (1990–2020) revealed a significant ($p < 0.001$) rising trend of NDVI with Kendall or Tau value of 0.47 with the highest z-score of 3.42 and Sen's slope of 0.004 followed by a significant ($p < 0.001$) declining trend of TGSI with Tau of – 0.54 with a z-score of −3.92 and negative Sen's slope of − 0.005. NDBaI also revealed a significant ($P < 0.01$) declining trend with Tau of −0.34, z-score of −2.48 and −0.001 Sens's value (Table 9). Hence, the three remote sensing indices presenting prominent land cover/land use of the region express a significant inverse relationship between them (Fig. 12).

Meteorological indices i.e., SPI-1, and SPI-6 revealed a significant ($P < 0.01$) trend while SPI-3 exposed a non-significant trend. The positive

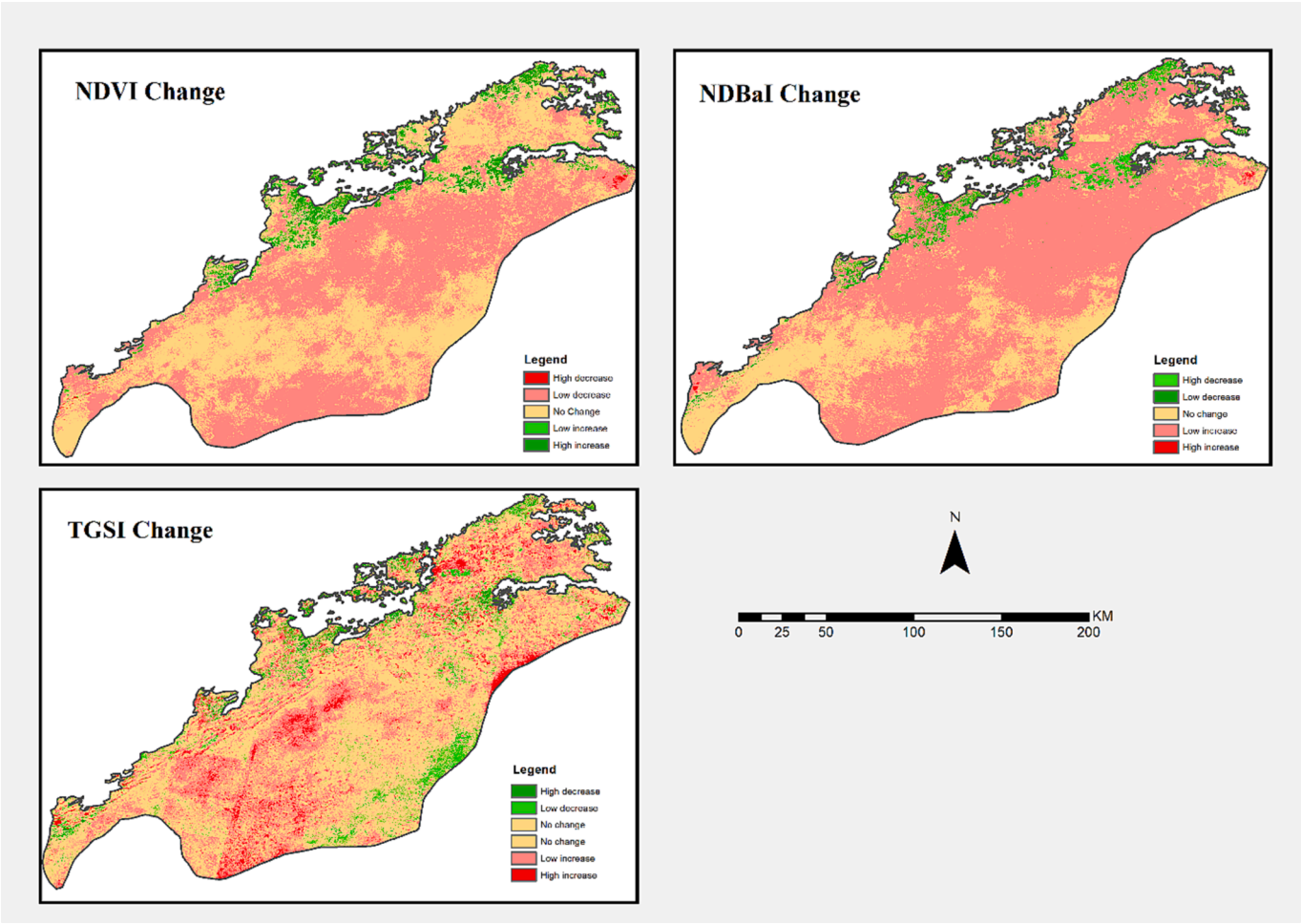

Fig. 10. Spatial pattern of index change detection of remote sensing indices from 1996 to 2020.

Table 8
Index-based change detection (NDVI-change, NDBaI-change, TGSI-change) 1996–2020.

Index	Change type	Area sq. km	Percentage
NDVI	High Decrease	164,331	0.22
	Low Decrease	35,962,500	48.50
	No Change	33,234,200	44.83
	Low Increase	1,971,790	2.66
	High Increase	2,793,160	3.76
NDBaI	High Decrease	2,017,120	2.72
	Low Decrease	2,482,960	3.34
	No Change	20,651,700	27.86
	Low Increase	48,873,300	65.93
	High Increase	100,908	0.13
TGSI	High Decrease	1,154,710	1.55
	Low Decrease	4,510,850	6.08
	No Change	41,811,700	56.40
	Low Increase	24,862,300	33.54
	High Increase	1,786,400	2.40

Sen's slope (0.017, 0.014, & 0.047) and z-score (1.68, 0.75, & 2.0) of three meteorological indices revealed the rising trend with positive SPI values (presenting low to no drought trend) in the region (Table 9).

3.4.2. *Pearson correlation and cross correlation analysis of all variables*

To examine the linear relationship between LCLU and meteorological drought variables, Pearson correlation revealed all significant positive and negative relationships between them (Fig. 13). First, the three prominent LCLU of the region namely vegetation (VEG), range land (RL) and barren land (BAR) exposed a high significant positive correlation of 0.79 with NDVI, and a high significant negative correlation of 0.9 with NDBaI and TGSI. Similarly, VEG & RL also exposed a significant negative correlation −0.6 and −0.82 with NDBaI and TGSI. Hence, NDVI, NDBaI and TGSI are found to be good representatives of prominent LCLU of the region (Fig. 13).

Moreover, different LCLU also revealed a significant relationship with meteorological indices e.g., NDVI had a significant correlation of 0.66 with SPI-3 and SPI-6 and 0.88 with SPI-1. It clearly indicates that the increasing trend of positive SPI values leads to an increase in vegetation of the region specifically in the form of agricultural land expansion. While a negative significant relationship between NDVI and drought frequency SPI-1, SPI-3, and SPI-6 (DFSPI-1, DFSPI-3, DFSPI-6) also revealed that more declining trend of DFSPI-3 and DFSPI-6 is increasing the NDVI in the region. A significant negative correlation of −0.58 and −0.48 is observed between NDVI and DFSPI-3 and 6 respectively (Fig. 13).

Cross correlation revealed that at lag 0, a strong positive correlation is observed between NDVI and SPI-1 (0.469), SPI-3 (0.592), and SPI-6 (0.693). Highest peak at lag 0 showed that two values are correlated without any time shift. For NDBaI and SPI, the highest peak is observed at lag + 14, indicating 2nd value follows the 1st value by 14 years revealing a time-dependent relationship. For TGSI, the highest peak is observed at lag −17 indicating 2nd value preceded the 1st value by 17 years (Fig. 14).

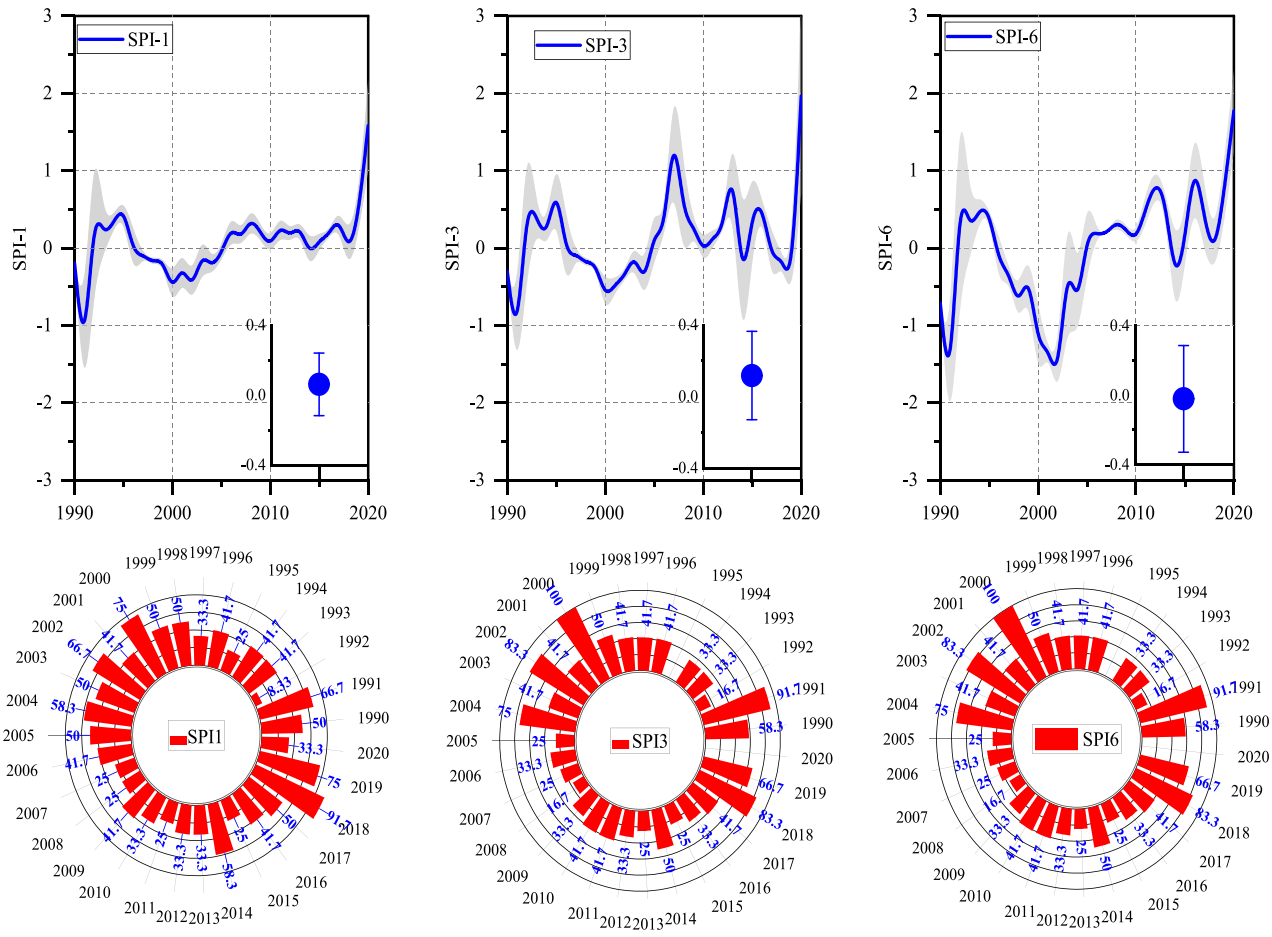

Fig. 11. A) time series of drought indices (spi-1, spi-3, and spi-6) from 1990 to 2020. b) Yearly drought frequency (in % months) from 1990 to 2020.

Table 9
Man-Kendall trend and Sen's slope of remote sensing and drought indices.

Variables	NDVI	NDBaI	TGSI	SPI-1	SPI-3	SPI-6
Tau	0.47***	− 0.34*	− 0.54***	0.23*	0.10	0.27*
z-score	3.42	− 2.48	−3.92	1.68	0.75	2.00
Sen's slope	0.004	− 0.001	−0.005	0.017	0.014	0.047
variance	2296	2300	2299	2298	2301	2301

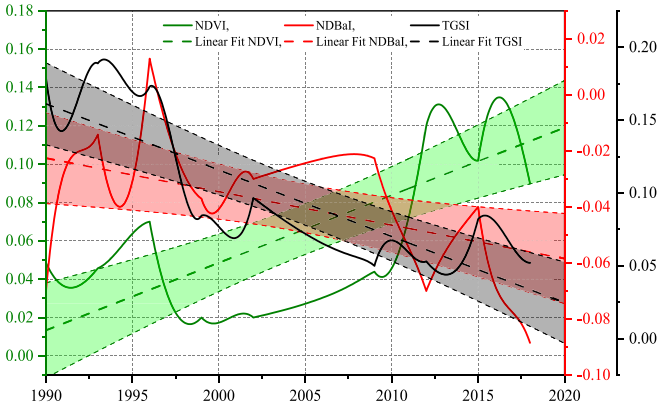

Fig. 12. Trend line detection of remote sensing indices (NDVI, NDBaI, and TGSI).

3.4.3. *Linear and non-linear regression between LCLU and meteorological indices*

Linear and polynomial regression revealed the strength of the relationship between LCLU representatives i.e., remote sensing indices and droughts indices (Fig. 15 and Table 10). Each of the remote sensing index i.e., NDVI, NDBaI, and TGSI are taken as separate dependent variables of SPI-1, SPI-3, and SPI-6. Results revealed that NDVI had a more strengthen relationship with meteorological droughts with linear and polynomial (cubic) R^2 followed by NDBaI and TGSI.

NDVI is highly predicted from SPI-6 with the highest linear and polynomial R^2 of 0.42 and 0.48 followed by SPI-1 with R^2 of 0.27 and 0.31 and SPI-3 with R^2 of 0.14 and 0.15. Further, NDBaI has a slightly better relationship with SPI-6 with linear and polynomial R^2 of 0.10 and 0.11 and Pearson correlation of 0.3. TGSI is observed to have a weak and non-significant relationship with SPI-6, SPI-1 and SPI-3 respectively (Table 10).

Overall, results derived from regression fit revealed that among all LCLU representatives, NDVI is observed to have the most significant relationship with meteorological droughts. Results also revealed that SPI-6 is the most significant predictor followed by SPI-1 and SPI-3.

4. Discussion

4.1. *Drivers of LCLU change*

LCLU change is more often driven by several biophysical (climate and extreme events) and human factors (demographic, institutional, and cultural) at local and regional scale (Achugbu et al., 2023; Roy and Rahman, 2023; Xie et al., 2022). For instance, Duraisamy et al. (2018)

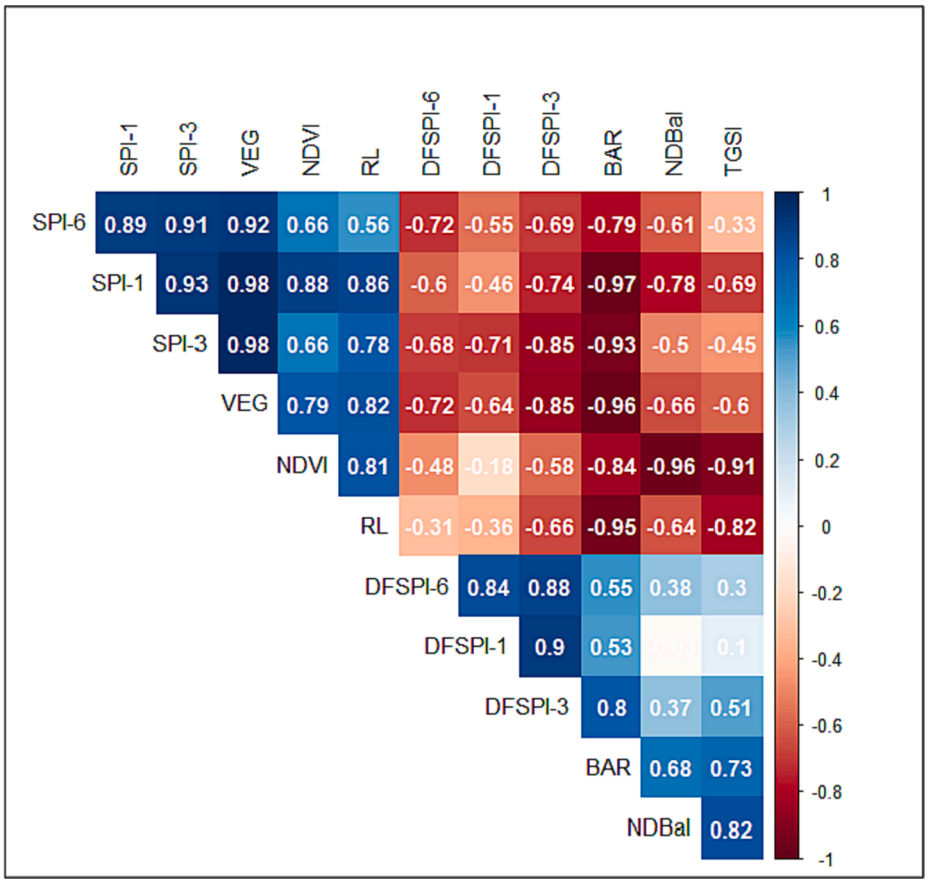

Fig. 13. Pearson correlation matrix of all LCLU and drought indicators.

reported a range of natural, institutional, technological, and economic factors for LCLU changes in a semi-arid region. However, climate driven modifications in LCLU lead to resource depletion and changes in ecosystem services (Xie et al., 2022). For example, Balist et al. (2021) projected a decline in water yield based on future climate scenarios and land use changes in arid river basin of Iran. Duan et al. (2019) also reported that high temperature and precipitation decline will exacerbate the situation of water deficit drought and challenge the food security nexus in central Asia. Uni or bidirectional changes in land use often occur at the expense of other land use. In deserted regions, rangelands (shrublands and grasslands) and barren lands are most responsible for significant conversions like cropland expansion (Cai et al., 2021). However, several climatic factors like temperature and precipitation are responsible for land degradation and land use conversions (Shoba and Ramakrishnan, 2016). For instance, Duan et al. (2020) also reported a substantial pressure on a lake water resource of central Asia due to climatic induced land use changes. The focus of our study also aimed to examine the climate induced LCLU changes in the extreme arid region of Pakistan in the past 3 decades. The major land use conversions in our studied region are attributed to the expansion of vegetation or agricultural land at the expense of other land use (Figs. 5 and 7). The results of our study are aligned with the study of Arshad et al., (2022a) in the same region reporting the agricultural land use expansion and barren land reduction. NDVI as a representative of vegetation land use showed an increasing trend and NDBaI as a representative of barren land use showed a decreasing trend (Table 9 and Fig. 12). The subsequent rise in NDVI is proportional to several climatic factors including temperature and precipitation (Ghebrezgabher et al., 2020; Shi et al., 2023). In the recent decades over Cholistan, the climate has generally become warmer and drier with unprecedented seasonal rainfall pattern (Hassan et al., 2019). Particularly, monsoon rains in summers and western disturbances in winters supported to maintain the required soil moisture of desert vegetation. A recent study by Wahla et al. (2023) evaluated climatic (temperature and precipitation) and human (population and GDP) as significant predictors of LCLU change in the Cholistan region. For instance, Arshad et al., (2022a) also discussed that advancement in irrigation system and local government support facilitated the expansion of subsistence agricultural activities in Cholistan at the expense of reduction in barren land. Hence, the substantial increase in NDVI, coupled with a reduction in bareness index (NDBaI), signifies an enhancement in vegetation conditions attributed to human agricultural practices. Moreover, the dynamics of LCLU change in this region is also associated with the settlement growth and urbanization at district level resulting an expansion of agricultural activities (Asif et al., 2023). Furthermore, the observed decrease in NDBaI i.e., bareness in the region linked with deliberate human interventions carries significant implication for environmental sustainability in desert ecosystem of Cholistan. To support the phenomenon, Government of Pakistan implemented a National Action Plan reported by Khan et al. (2013) addressing the mitigation strategies to combat desertification and sustainable land use practices in Cholistan. These fundamental changes in land use conversions of the desert would provide significant ecological benefits such as improved biodiversity and habitat resources for local flora and fauna, soil stability with less erosion risk and supporting carbon sequestration.

Overall, the expansion of agricultural land areas in arid or deserted regions to meet food demands and achieve the goal of food security has become a point of interest in several regions of the world (Elbeih, 2021; Moghazy and Kaluarachchi, 2020; Wang et al., 2022). For instance, Aziz (2021) also predicted an increase in the cropland area of Pakistan at the expense of a decrease in deserted barren land and grassland under future climate change scenarios. On contrary, another study by Samie et al. (2017) reported an expansion of built-up land area at the expense of

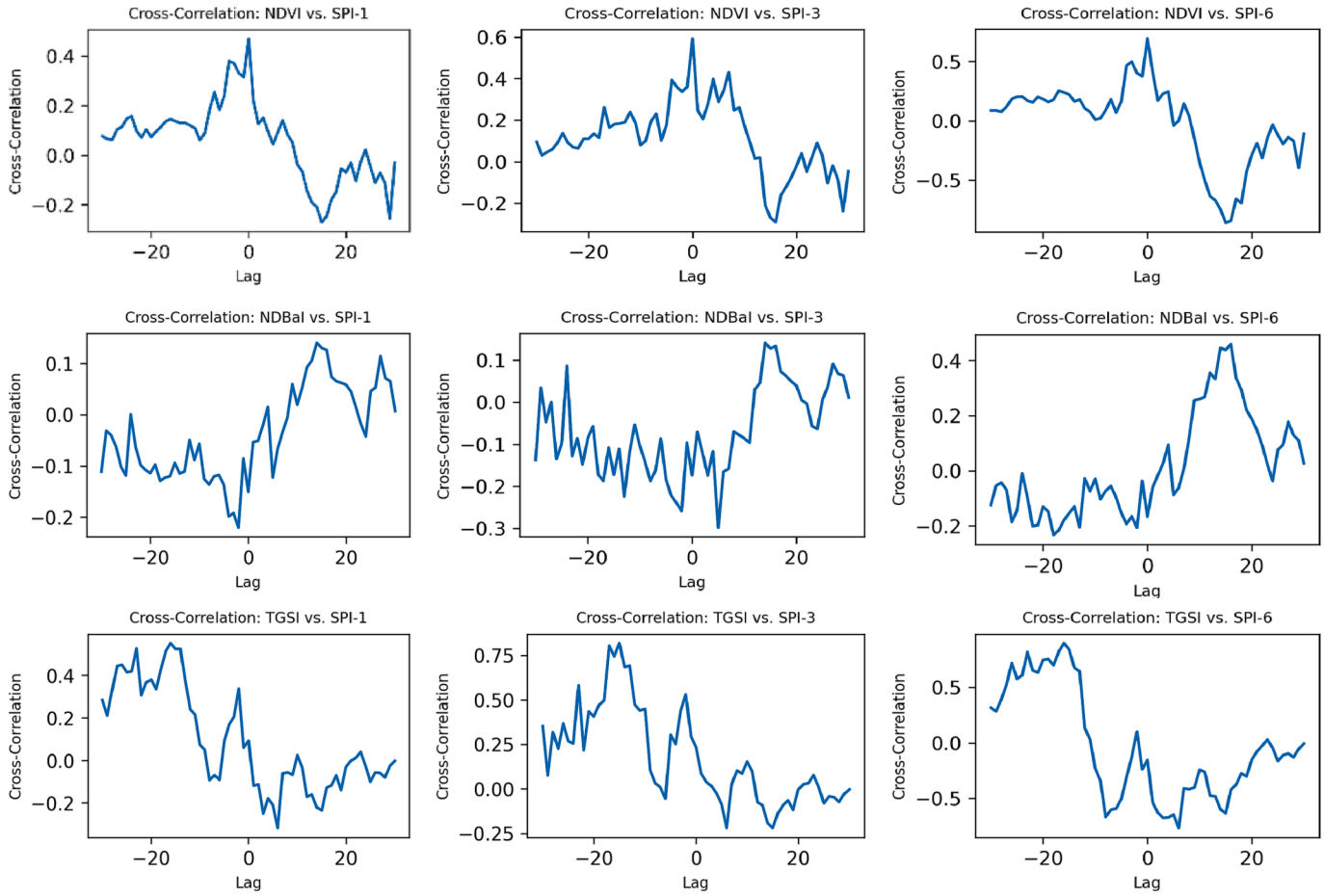

Fig. 14. Potential lag effect between drought events (SPI-1, SPI-3, and SPI-6) and Indices (NDVI, NDBaI, and TGSI).

barren or unused land at the provincial scale in Pakistan. Our study region belongs to the southern Punjab in Pakistan where agriculture is the major economic activity of the marginal population, and most of the human labor is consumed in crop farming and livestock rearing. Dryland agricultural landholdings of the region have moderate to developed adaptive capacity from climatic change to meet their goals of agricultural development (Mazhar et al., 2021). Established canal system, advancement in irrigation facilities, fertilization and suitability of climatic conditions are considered as main drivers of vegetation expansion in this region (Arshad et al., 2022a). Despite all technological development and favorable conditions, several dynamics of LCLU are being observed during the studied time of 3 decades. e.g., loss of vegetation at one timescale (2002 and 2014) and gain in another timescale (2008 and 2020) is attributed to extreme events like droughts.

4.2. *Impacts of meteorological droughts on LCLU changes*

Among various climatic factors, precipitation is the main deriving force in shaping the landscape structure of deserted regions (Ding and Xingming, 2021). Pakistan experienced several long- and short-term drought spells in previous decades attributed to El-Nino Southern Oscillations (ENSO) with extreme severity in southern arid regions (Saleem et al., 2021). The largest drought spell of the previous decade identified in this region was from 1998 to 2004 caused severe stress on vegetation and crop productivity (Arshad et al., 2023). The drought identification years of our results (Fig. 11) are aligned with several previous findings of the same drought spells during the EL-Nino phase (de Oliveira-Júnior et al., 2022; Ullah et al., 2022). During EL-Nino years, sea surface temperatures in the Pacific Ocean become warmer than usual, which causes changes in atmospheric circulation and precipitation patterns around the region. The 1997–1998 EL-Nino was one of the strongest on record and is believed to cause this severe drought spell in the region (Hina et al., 2021; Ullah et al., 2021). However, the recent drought spell of 2018 is not strongly induced by EL-Nino effects but related to the factors of high temperature, below-average rainfall, and inefficient water management practices in the region. Overall, the linear trend analysis (Mann-Kendall and Sen's slope) of our findings revealed an improvement or increase in vegetation and NDVI of the deserted region and a reduction in barren land (NDBaI and TGSI) of the region reflecting the technological and agricultural development in the region (Table 8 and Fig. 11). But our research findings also revealed a high correlation between LCLU area (vegetation, barren, and rangeland) and LCLU indices (NDVI, NDBaI, and TGSI) with meteorological droughts (SPI-1, SPI-3, and SPI-6) in the region (Fig. 13). It clearly depicts that drought years i.e., 2002 and 2014 had low NDVI with less vegetation area and high NDBaI and large barren land and wet years i.e., 2008 and 2020 had improved NDVI and more vegetation area at the expense of barren land indices (NDBaI and TGSI). Moreover, cross correlation also proved that positive correlations at various lags suggest that there is a relationship between NDVI and SPI (Fig. 14). It indicates that changes in vegetation health are associated with subsequent changes in drought conditions. The lag values for NDBaI and TGSI indicate delayed responses, with barrenness changes following meteorological drought events, emphasizing the importance of considering time lags in understanding the intricate dynamics between climatic factors and land use alterations. The correlation results are aligned with several other studies which report the impacts of meteorological droughts on NDVI of the regions (Li et al., 2019; Li et al., 2021; Nanzad et al., 2019). Along with linear relationship, polynomial regression provided a more better understanding of non-linear relationship between SPI and NDVI (Table 10 and

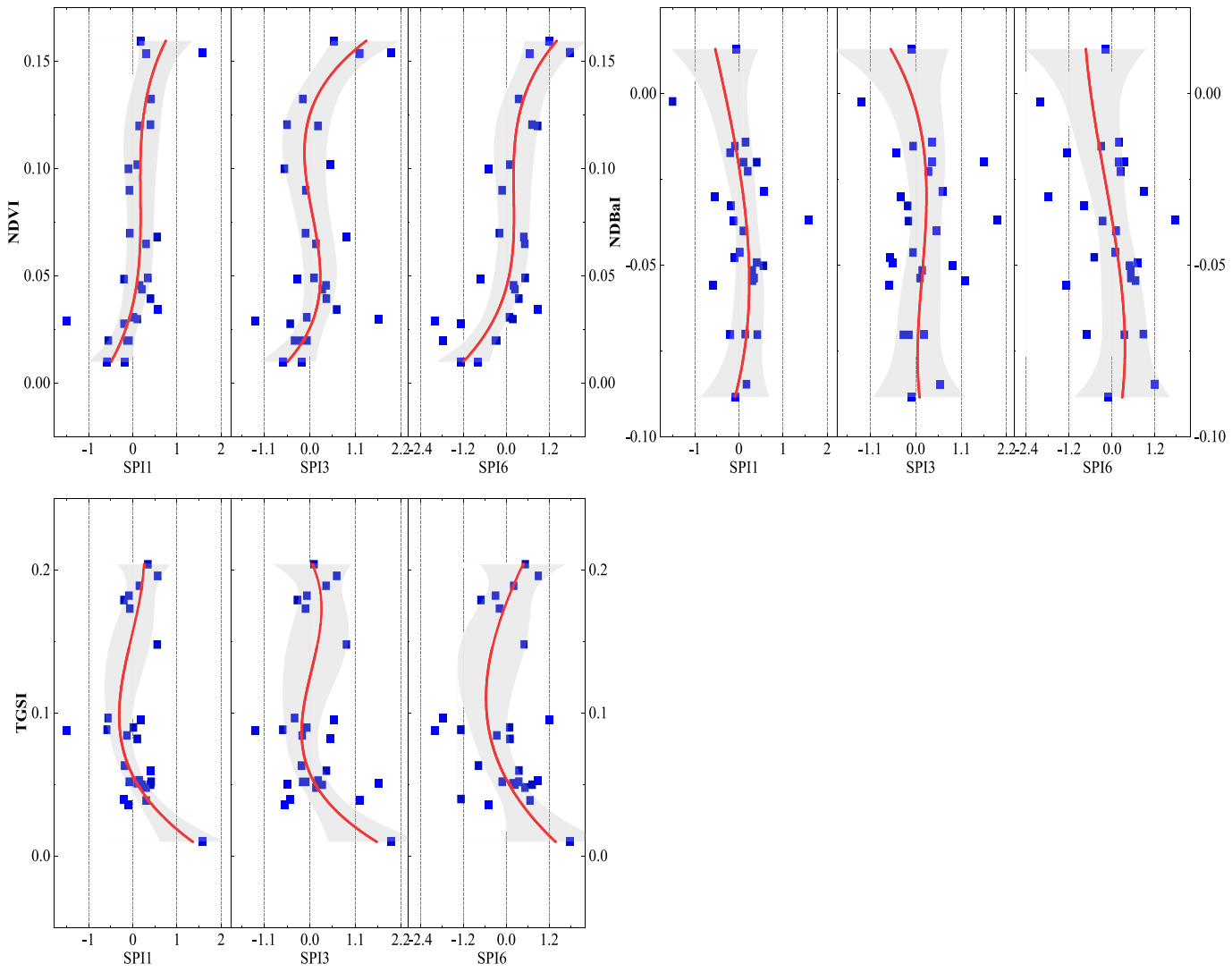

Fig. 15. Polynomial (cubic) trend fitting to predict dependent LCLU representatives (NDVI, NDBaI, and TGSI) from independent drought indices (SPI-1, SPI-3, and SPI-6).

Fig. 15) as also previously explored by Javed et al. (2020).

A recent study by Arshad et al., (2022b) in the same arid region also reported a moderately significant relationship between SPI and NDVI. Similarly, another study by Ashraf et al. (2022) also examined the linear temporal relationship between meteorological drought indices (SPI and RDI) and remote sensing vegetation indices (NDVI and EVI) in arid and agricultural regions of Pakistan. However, our study also reported the linear and non-linear (cubic polynomial) relationship between all LCLU indices (NDVI, NDBaI, and TGSI) with all drought indices (SPI-1, SPI-3, and SPI-6). Among LCLU indices, NDVI was found to be more strongly influenced by drought indices while NDBaI and TGSI have a weak linear and moderate non-linear relationship with best fit at cubic polynomial fit. Moreover, SPI-6 had a greater a influence in deriving LCLU characteristics of the deserted region followed by SPI-3. Overall, our study provided a meaningful approach to address LCLU changes in extreme arid deserted regions due to extreme events like meteorological droughts.

5. Limitations

It has been revealed, though the findings of our study provided meaningful insight about climatic driven LCLU changes in the desert ecosystem of Pakistan.

Despite correlated results of LCLU and drought indices, the study was also bounded to some other limitations and provides an extended future research direction. First, LCLU changes of this deserted region can be compared to other deserts of Pakistan like Thal in central Punjab and Thar in Sindh for more appropriate generalizations. Second, we used only precipitation based meteorological drought index (SPI) to address the influence of climatic extremes in LCLU changes of the region. Future research could examine the socio-economic factors that influence modifications in land use. Additional environmental factors such as temperature, relative humidity or evapotranspiration might be considered to enhance the analysis and provide information for decision-making. Drought occurrence is a cyclic phenomenon in this region due to ENSO with multiple linear and non-linear impacts on vegetation characteristics of the region which should be analyzed by comparing multiple statistical approaches. NDVI of the regions is more highly influenced by drought indices compared to NDBaI and TGSI. The results provide a future approach to predicting NDVI of the region from multiple climatic factors using modern machine learning based linear and non-linear algorithms.

6. Conclusion

This study has revealed interesting patterns of land use and land

Table 10
Linear and non-linear (polynomial) statistical inferences of remote sensing and drought indices.

var	Equation	Polynomial (cubic) R^2	Pearson correlation R	Linear R^2
NDVI vs SPI-1	(0.059) + 0.070(SPI-1) + 0.012(SPI-1)^2 – 0.013 (SPI-1)^3	0.31	0.56	0.27
NDVI vs SPI-3	(0.062) + 0.023(SPI-3) + 0.002(SPI-3)^2 + 0.001 (SPI-3)^3	0.15	0.39	0.14
NDVI vs SPI-6	(0.058) + 0.042(SPI-6) + 0.011(SPI-6)^2 – 0.001 (SPI-6)^3	0.48	0.69	0.42
NDBaI vs SPI-1	(-0.042) – 0.008(SPI-1) + 0.009(SPI-1)^2 – 0.001(SPI-1)^3	0.12	0.31	0.04
NDBaI vs SPI-3	(-0.045) – 0.002(SPI-3) + 0.013(SPI-3)^2 – 0.005(SPI-3)^3	0.08	0.28	0.02
NDBaI vs SPI-6	(-0.042) – 0.007(SPI-6) + 0.001(SPI-6)^2 —0.001(SPI-6)^3	0.11	0.33	0.10
TGSI vs SPI-1	(0.096) + 0.018(SPI-1) – 0.015(SPI-1)^2 – 0.017(SPI-1)^3	0.07	0.26	0.01
TGSI vs SPI-3	(0.10) + 0.03(SPI-3) – 0.011(SPI_3)^2 – 0.017 (SPI-3)^3	0.17	0.41	0.09
TGSI vs SPI-6	(0.10) + 0.006(SPI-6) – 0.015(SPI-6)^2 – 0.007(SPI-6)^3	0.07	0.27	0.04

cover changes from random forest supervised classification in the desert ecosystem of Pakistan during the last three decades. Three significant change detection techniques i.e., area percent change, post classification change, and index-based change all revealed a decline in barren land and increase in vegetative or agricultural land use of the desert which remained highly dependent upon climatic indicators during the decades.

Based on the study, the following major conclusions have been drawn:

1. The desert experienced significant LCLU change over 3 decades with the most significant expansion of vegetation or agricultural land at the expense of barren land. The highest vegetation expansion (4.4 %) took place from 2014 to 2020 at the expense of the highest reduction of barren land (-6.3 %). Furthermore, post classification change detection also revealed most of the interconversions between barren, rangeland, and vegetative or agricultural land of the desert with 95047 ha conversion of barren to vegetation. Index based change detection presents a competitive interplay between three LCLU representatives (NDVI, NDBaI, and TGSI), whereas 6.4 % increase in NDVI is associated with 6 % decrease in NDBaI, and 7.5 % decrease in TGSI.
2. Desert experienced 11 droughts years in the past 3 decades with significant impacts on LCLU of the region. Drought's years (2002 and 2014) experienced a loss of vegetation area at the rate of −1% and with low NDVI, high NDBaI and TGSI in the region. Mann-Kendall trend analysis also showed a significant decline in barrenness from NDBaI and TGSI (SS = -0.001, −0.005) and rise in NDVI (SS = 0.004) with subsequent rise in SPI-1, SPI-3, and SPI-6 (SS = 0.01 and 0.04).
3. LCLU classes and indices (NDVI, NDBaI, and TGSI) are highly correlated with SPI-1, SPI-3 and SPI-6 in the selected years of LCLU change analysis. SPI-1,3, and 6 are found to have a significant positive correlation range (r = 0.6–0.8) with NDVI, negative correlation range (r = 0.5–0.7) with NDBaI, and (r = 0.3–0.6) with TGSI. Negative correlation range (r = 0.4–0.5) between drought frequency DFSPI-3, and 6 with NDVI clearly shows that temporal decrease in drought frequency facilitated the improvement of desert greenness in the selected season of LCLU change analysis. Furthermore, improved polynomial relationship between LCLU indices and drought indices shows NDVI (R^2 = 0.3 and 0.4) to be the highly significant predictor of SPI-1 and SPI-6.

Hereafter, findings from the study proved that LCLU of the 2nd largest desert of the country is significantly driven by the frequent occurrence of extreme events i.e., droughts. Overall, the increase in vegetation (NDVI) and reduction of barrenness (NDBaI) enhanced ecosystem resilience by fostering increased biodiversity, improving soil stability, and promoting sustainable agricultural practices. However, LCLU of the region is also vulnerable to climatic change and is highly influenced by meteorological drought (SPI). Overall, the study provides a baseline approach to comprehend the impacts of climatic change on LCLU of the region for better adaptation strategies in the future.

CRediT authorship contribution statement

Zulqadar Faheem: Conceptualization, Writing – review & editing. **Jamil Hasan Kazmi:** Writing – review & editing. **Saima Shaikh:** Writing – review & editing. **Sana Arshad:** Conceptualization, Data curation, Formal analysis, Methodology, Writing – original draft. **Noreena:** Data curation, Writing – review & editing. **Safwan Mohammed:** Methodology, Formal analysis, Visualization, Validation, Writing – review & editing, Funding acquisition.

Declaration of competing interest

The authors declare that they have no known competing financial interests or personal relationships that could have appeared to influence the work reported in this paper.

Data availability

Data will be made available on request.

Acknowledgements

Safwan Mohammed was supported the TKP2021-NKTA-32 project, funded by the National Research Development and Innovation Fund, under the TKP2021-NKTA call for proposals.

References

Abdullah, M., Rafay, M., Sial, N., Rasheed, F., Nawaz, M., Nouman, W., Ahmad, I., Ruby, T., Khalil, S., 2017. Determination of forage productivity, carrying capacity and palatability of browse vegetation in arid rangelands of cholistan desert (pakistan). Appl. Ecol. Environ. Res. 15, 623–637.

Achugbu, I.C., Laux, P., Olufayo, A.A., Balogun, I.A., Dudhia, J., Arnault, J., Gbode, I.E., Naabil, E., Kunstmann, H., 2023. The impacts of land use and land cover change on biophysical processes in West Africa using a regional climate model experimental approach. Int. J. Climatol. 43, 1731–1755.

Ajani, A., van der Geest, K., 2021. Climate change in rural Pakistan: evidence and experiences from a people-centered perspective. Sustain. Sci. 16, 1999–2011.

Akram, M., Kahlown, M.A., Soomro, Z.A., 2008. Desertification Control for Sustainable Land Use in the Cholistan Desert, Pakistan. In: Lee, C., Schaaf, T. (Eds.), The Future of Drylands. Springer, Netherlands, Dordrecht, pp. 483–492.

Alem, A., Kumar, S., 2022. Transfer Learning Models for Land Cover and Land Use Classification in Remote Sensing Image. Appl. Artif. Intell. 36, 2014192.

Al-Quraishi, A.M.F., Qader, S.H., Wu, W., 2020. Drought Monitoring Using Spectral and Meteorological Based Indices Combination: A Case Study in Sulaimaniyah, Kurdistan Region of Iraq. In: Al-Quraishi, A.M.F., Negm, A.M. (Eds.), Environmental Remote Sensing and GIS in Iraq. Springer International Publishing, Cham, pp. 377–393.

Arshad, S., Hasan Kazmi, J., Fatima, M., Khan, N., 2022a. Change detection of land cover/land use dynamics in arid region of Bahawalpur District, Pakistan. Applied Geomatics 14, 387–403.

Arshad, S., Kazmi, J.H., Shaikh, S., Fatima, M., Faheem, Z., Asif, M., Arshad, W., 2022b. Geospatial assessment of early summer heatwaves, droughts, and their relationship with vegetation and soil moisture in the arid region of Southern Punjab, Pakistan. J. Water Clim. Change 13, 4105–4129.

Arshad, S., Kazmi, J.H., Prodhan, F.A., Mohammed, S., 2023. Exploring dynamic response of agrometeorological droughts towards winter wheat yield loss risk using

machine learning approach at a regional scale in Pakistan. Field Crop Res 302, 109057.
Arshad, M., Ma, X., Yin, J., Ullah, W., Liu, M., Ullah, I., 2021. Performance evaluation of ERA-5, JRA-55, MERRA-2, and CFS-2 reanalysis datasets, over diverse climate regions of Pakistan. Weather Clim. Extremes 33, 100373.
Arshad, A., Zhang, W., Zaman, M.A., Dilawar, A., Sajid, Z., 2019. Monitoring the impacts of spatio-temporal land-use changes on the regional climate of city Faisalabad, Pakistan. Ann. GIS 25, 57–70.
Ashraf, M., Ullah, K., Adnan, S., 2022. Satellite based impact assessment of temperature and rainfall variability on drought indices in Southern Pakistan. Int. J. Appl. Earth Obs. Geoinf. 108, 102726.
Asif, M., Kazmi, J.H., Tariq, A., Zhao, N., Guluzade, R., Soufan, W., Almutairi, K.F., Sabagh, A.E., Aslam, M., 2023. Modelling of land use and land cover changes and prediction using CA-Markov and Random Forest. Geocarto Int. 38, 2210532.
Aziz, T., 2021. Changes in land use and ecosystem services values in Pakistan, 1950–2050. Environ. Dev. 37, 100576.
Balist, J., Malekmohammadi, B., Jafari, H.R., Nohegar, A., Geneletti, D., 2021. Detecting land use and climate impacts on water yield ecosystem service in arid and semi-arid areas. A study in Sirvan River Basin-Iran. Appl. Water Sci. 12, 4.
Bera, D., Chatterjee, N.D., Bera, S., 2021. Comparative performance of linear regression, polynomial regression and generalized additive model for canopy cover estimation in the dry deciduous forest of West Bengal. Remote Sens. Appl.: Soc. Environ. 22, 100502.
Bhatti, M.T., Anwar, A.A., Hussain, K., 2023. Characterization and outlook of climatic hazards in an agricultural area of Pakistan. Sci. Rep. 13, 9958.
Biazin, B., Sterk, G., 2013. Drought vulnerability drives land-use and land cover changes in the Rift Valley dry lands of Ethiopia. Agr Ecosyst Environ 164, 100–113.
Bradley, R.A., Srivastava, S.S., 1979. Correlation in Polynomial Regression. Am. Stat. 33, 11–14.
Burrell, A.L., Evans, J.P., De Kauwe, M.G., 2020. Anthropogenic climate change has driven over 5 million km2 of drylands towards desertification. Nat. Commun. 11, 3853.
Cai, T., Zhang, X., Xia, F., Zhang, Z., Yin, J., Wu, S., 2021. The Process-Mode-Driving Force of Cropland Expansion in Arid Regions of China Based on the Land Use Remote Sensing Monitoring Data. Remote Sens. (Basel) 13, 2949.
Chen, W., Di, K., Cai, Q., Li, D., Liu, C., 2023. Research on Motivational Mechanisms and Pathways for Promoting Public Participation in Environmental Protection Behavior. Int. J. Environ. Res. Public Health 20, 5084.
Chen, D., Loboda, T.V., Hall, J.V., 2020. A systematic evaluation of influence of image selection process on remote sensing-based burn severity indices in North American boreal forest and tundra ecosystems. ISPRS J. Photogramm. Remote Sens. 159, 63–77.
Chughtai, A.H., Abbasi, H., Karas, I.R., 2021. A review on change detection method and accuracy assessment for land use land cover. Remote Sens. Appl.: Soc. Environ. 22, 100482.
Costa, L.C., Martins do Amaral Cunha, A.P., Anderson, L.O., Cunningham, C., 2021. New approach for drought assessment: A case study in the northern region of Minas Gerais. Int. J. Disaster Risk Reduct. 53, 102019.
Damaneh, E.H., Damaneh, E.H., Khosravi, H., Gholami, H., 2019. Analysis and monitoring of drought using NDVI index (Case study: the west basin of Jaz Murian wetland). J. Rangeland 13, 461–475.
Daramola, M.T., Xu, M., 2022. Recent changes in global dryland temperature and precipitation. Int. J. Climatol. 42, 1267–1282.
de Barros de Sousa, L., de Assunção Montenegro, A.A., da Silva, M.V., Almeida, T.A.B., de Carvalho, A.A., da Silva, T.G.F., de Lima, J.L.M.P., 2023. Spatiotemporal Analysis of Rainfall and Droughts in a Semiarid Basin of Brazil: Land Use and Land Cover Dynamics. Remote Sens. (Basel) 15, 2550.
de Oliveira-Júnior, J.F., Shah, M., Abbas, A., Iqbal, M.S., Shahzad, R., de Gois, G., da Silva, M.V., da Rosa Ferraz Jardim, A.M., de Souza, A., 2022. Spatiotemporal analysis of drought and rainfall in Pakistan via Standardized Precipitation Index: homogeneous regions, trend, wavelet, and influence of El Niño-southern oscillation. Theor. Appl. Climatol. 149, 843–862.
Di, K., Chen, W., Zhang, X., Shi, Q., Cai, Q., Li, D., Liu, C., Di, Z., 2023. Regional unevenness and synergy of carbon emission reduction in China's green low-carbon circular economy. J. Clean. Prod. 420, 138436.
Ding, H., Xingming, H., 2021. Spatiotemporal change and drivers analysis of desertification in the arid region of northwest China based on geographic detector. Environmental Challenges 4, 100082.
Duan, W., Chen, Y., Zou, S., Nover, D., 2019. Managing the water-climate- food nexus for sustainable development in Turkmenistan. J. Clean. Prod. 220, 212–224.
Duan, W., Zou, S., Chen, Y., Nover, D., Fang, G., Wang, Y., 2020. Sustainable water management for cross-border resources: The Balkhash Lake Basin of Central Asia, 1931–2015. J. Clean. Prod. 263, 121614.
Duraisamy, V., Bendapudi, R., Jadhav, A., 2018. Identifying hotspots in land use land cover change and the drivers in a semi-arid region of India. Environ. Monit. Assess. 190, 535.
Elbeih, S.F., 2021. Evaluation of agricultural expansion areas in the Egyptian deserts: A review using remote sensing and GIS. Egypt. J. Remote Sens. Space Sci. 24, 889–906.
Feng, S., Li, W., Xu, J., Liang, T., Ma, X., Wang, W., Yu, H., 2022b. Land Use/Land Cover Mapping Based on GEE for the Monitoring of Changes in Ecosystem Types in the Upper Yellow River Basin over the Tibetan Plateau. Remote Sens. (Basel) 14, 5361.
Feng, K., Wang, T., Liu, S., Kang, W., Chen, X., Guo, Z., Zhi, Y., 2022a. Monitoring Desertification Using Machine-Learning Techniques with Multiple Indicators Derived from MODIS Images in Mu Us Sandy Land. China. Remote Sensing 14, 2663.
Fensholt, R., Langanke, T., Rasmussen, K., Reenberg, A., Prince, S.D., Tucker, C., Scholes, R.J., Le, Q.B., Bondeau, A., Eastman, R., Epstein, H., Gaughan, A.E., Hellden, U., Mbow, C., Olsson, L., Paruelo, J., Schweitzer, C., Seaquist, J., Wessels, K., 2012. Greenness in semi-arid areas across the globe 1981–2007 — an Earth Observing Satellite based analysis of trends and drivers. Remote Sens. Environ. 121, 144–158.
Fu, Q., Li, B., Hou, Y., Bi, X., Zhang, X., 2017. Effects of land use and climate change on ecosystem services in Central Asia's arid regions: A case study in Altay Prefecture, China. Sci. Total Environ. 607–608, 633–646.
Fung, T., LeDrew, E., 1988. For change detection using various accuracy. Photogramm. Eng. Remote Sens 54, 1449–1454.
Gaikwad, S.V., Vibhute, A.D., Kale, K.V., 2022. Assessing Meteorological Drought and Detecting LULC Dynamics at a Regional Scale Using SPI, NDVI, and Random Forest Methods. SN Computer Science 3, 458.
Ge, G., Shi, Z., Zhu, Y., Yang, X., Hao, Y., 2020. Land use/cover classification in an arid desert-oasis mosaic landscape of China using remote sensed imagery: Performance assessment of four machine learning algorithms. Global Ecol. Conserv. 22, e00971.
Ge, G., Zhang, J., Chen, X., Liu, X., Hao, Y., Yang, X., Kwon, S., 2022. Effects of land use and land cover change on ecosystem services in an arid desert-oasis ecotone along the Yellow River of China. Ecol. Eng. 176, 106512.
Gelaro, R., McCarty, W., Suárez, M.J., Todling, R., Molod, A., Takacs, L., Randles, C.A., Darmenov, A., Bosilovich, M.G., Reichle, R., Wargan, K., Coy, L., Cullather, R., Draper, C., Akella, S., Buchard, V., Conaty, A., da Silva, A.M., Gu, W., Kim, G.-K., Koster, R., Lucchesi, R., Merkova, D., Nielsen, J.E., Partyka, G., Pawson, S., Putman, W., Rienecker, M., Schubert, S.D., Sienkiewicz, M., Zhao, B., 2017. The Modern-Era Retrospective Analysis for Research and Applications, Version 2 (MERRA-2). J. Clim. 30, 5419–5454.
Gertner, G., Wang, G., Fang, S., Anderson, A.B., 2002. Mapping and uncertainty of predictions based on multiple primary variables from joint co-simulation with Landsat TM image and polynomial regression. Remote Sens. Environ. 83, 498–510.
Ghebrezgabher, M.G., Yang, T., Yang, X., Eyassu Sereke, T., 2020. Assessment of NDVI variations in responses to climate change in the Horn of Africa. Egypt. J. Remote Sens. Space Sci. 23, 249–261.
Halmy, M.W.A., Gessler, P.E., Hicke, J.A., Salem, B.B., 2015. Land use/land cover change detection and prediction in the north-western coastal desert of Egypt using Markov-CA. Appl. Geogr. 63, 101–112.
Hassan, I., Ghumman, A., Aruba, W., 2019. Simulating precipitation of Bahawalpur and its adjoining Cholistan desert of Pakistandue to climate change. Int. J. Water Resour. Arid. Environ 8, 109–117.
He, L., Guo, J., Yang, W., Jiang, Q., Chen, L., Tang, K., 2023. Multifaceted responses of vegetation to average and extreme climate change over global drylands. Sci. Total Environ. 858, 159942.
He, B., Wang, S., Guo, L., Wu, X., 2019. Aridity change and its correlation with greening over drylands. Agric. For. Meteorol. 278, 107663.
Heidari, S., Shamsipour, A., Kakroodi, A.A., Bazgeer, S., 2023. Monitoring land cover changes and droughts using statistical analysis and multi-sensor remote sensing data. Environ. Monit. Assess. 195, 618.
Hina, S., Saleem, F., Arshad, A., Hina, A., Ullah, I., 2021. Droughts over Pakistan: possible cycles, precursors and associated mechanisms. Geomat. Nat. Haz. Risk 12, 1638–1668.
Hussain, S., Mubeen, M., Akram, W., Ahmad, A., Habib-ur-Rahman, M., Ghaffar, A., Amin, A., Awais, M., Farid, H.U., Farooq, A., Nasim, W., 2019. Study of land cover/land use changes using RS and GIS: a case study of Multan district. Pakistan. Environmental Monitoring and Assessment 192, 2.
Hussain, S., Mubeen, M., Ahmad, A., Majeed, H., Qaisrani, S.A., Hammad, H.M., Amjad, M., Ahmad, I., Fahad, S., Ahmad, N., Nasim, W., 2022. Assessment of land use/land cover changes and its effect on land surface temperature using remote sensing techniques in Southern Punjab, Pakistan. Environmental Science and Pollution Research.
Ijaz, M., Zafar, Q., Khan, A.A., Hassan, S.S., 2023. Assessing drought and its impacts on wheat yield using remotely sensed observations in rainfed Potohar region of Pakistan. Environ. Dev. Sustain. 25, 3699–3721.
Javed, T., Yao, N., Chen, X., Suon, S., Li, Y., 2020. Drought evolution indicated by meteorological and remote-sensing drought indices under different land cover types in China. Environ. Sci. Pollut. Res. 27, 4258–4274.
Kendall, M.G., 1948. Rank correlation methods.
Khan, A., Ahmad, D.M., Shah Hashmi, H., 2013. Review of available knowledge on land degradation in Pakistan. USAID.
Kleemann, J., Baysal, G., Bulley, H.N.N., Fürst, C., 2017. Assessing driving forces of land use and land cover change by a mixed-method approach in north-eastern Ghana, West Africa. J. Environ. Manage. 196, 411–442.
Li, G., Sun, S., Han, J., Yan, J., Liu, W., Wei, Y., Lu, N., Sun, Y., 2019. Impacts of Chinese Grain for Green program and climate change on vegetation in the Loess Plateau during 1982–2015. Sci. Total Environ. 660, 177–187.
Li, P., Wang, J., Liu, M., Xue, Z., Bagherzadeh, A., Liu, M., 2021. Spatio-temporal variation characteristics of NDVI and its response to climate on the Loess Plateau from 1985 to 2015. Catena 203, 105331.
Liu, Z., Wang, Y., Shao, M., Jia, X., Li, X., 2016. Spatiotemporal analysis of multiscalar drought characteristics across the Loess Plateau of China. J. Hydrol. 534, 281–299.
Lloyd-Hughes, B., Saunders, M.A., 2002. A drought climatology for Europe. Int. J. Climatol. 22, 1571–1592.
Lu, X., Wang, L., McCabe, M.F., 2016. Elevated CO2 as a driver of global dryland greening. Sci. Rep. 6, 20716.
Majeed, M., Tariq, A., Anwar, M.M., Khan, A.M., Arshad, F., Mumtaz, F., Farhan, M., Zhang, L., Zafar, A., Aziz, M., Abbasi, S., Rahman, G., Hussain, S., Waheed, M., Fatima, K., Shaukat, S., 2021. Monitoring of Land Use-Land Cover Change and Potential Causal Factors of Climate Change in Jhelum District, Punjab, Pakistan, through GIS and Multi-Temporal Satellite Data. Land 10, 1026.

Mann, H.B., 1945. Nonparametric tests against trend. Econometrica 3, 245–259.
Martínez-Valderrama, J., Guirado, E., Maestre, F.T., 2020. Desertifying Deserts. Nature Sustainability 3, 572–575.
Mateen, S., Nuthammachot, N., Techato, K., Ullah, N., 2023. Billion Tree Tsunami Forests Classification Using Image Fusion Technique and Random Forest Classifier Applied to Sentinel-2 and Landsat-8 Images: A Case Study of Garhi Chandan Pakistan. ISPRS Int. J. Geo Inf. 12, 9.
Mawenda, J., Watanabe, T., Avtar, R., 2020. An Analysis of Urban Land Use/Land Cover Changes in Blantyre City, Southern Malawi (1994–2018). Sustainability 12, 2377.
Mazhar, N., Shirazi, S.A., Stringer, L.C., Carrie, R.H., Dallimer, M., 2021. Spatial patterns in the adaptive capacity of dryland agricultural households in South Punjab. Pakistan. Journal of Arid Environments 194, 104610.
McCluney, K.E., Belnap, J., Collins, S.L., González, A.L., Hagen, E.M., Nathaniel Holland, J., Kotler, B.P., Maestre, F.T., Smith, S.D., Wolf, B.O., 2012. Shifting species interactions in terrestrial dryland ecosystems under altered water availability and climate change. Biol. Rev. 87, 563–582.
Mckee, T., Doesken, N., Kleist, J., 1993. The relationship of drought frequency and duration to time scales. Applied Climatology 17, 179–183.
Mihi, A., Ghazela, R., wissal, D.,, 2022. Mapping potential desertification-prone areas in North-Eastern Algeria using logistic regression model, GIS, and remote sensing techniques. Environ. Earth Sci. 81, 385.
Moghazy, N.H., Kaluarachchi, J.J., 2020. Sustainable Agriculture Development in the Western Desert of Egypt: A Case Study on Crop Production, Profit, and Uncertainty in the Siwa Region. Sustainability 12, 6568.
Moisa, M.B., Gabissa, B.T., Hinkosa, L.B., Dejene, I.N., Gemeda, D.O., 2022. Analysis of land surface temperature using Geospatial technologies in Gida Kiremu, Limu, and Amuru District, Western Ethiopia. Artificial Intelligence in Agriculture 6, 90–99.
Nanzad, L., Zhang, J., Tuvdendorj, B., Nabil, M., Zhang, S., Bai, Y., 2019. NDVI anomaly for drought monitoring and its correlation with climate factors over Mongolia from 2000 to 2016. J. Arid Environ. 164, 69–77.
Opedes, H., Mücher, S., Baartman, J.E.M., Nedala, S., Mugagga, F., 2022. Land Cover Change Detection and Subsistence Farming Dynamics in the Fringes of Mount Elgon National Park, Uganda from 1978–2020. Remote Sens. (Basel) 14, 2423.
Peiman, R., 2011. Pre-classification and post-classification change-detection techniques to monitor land-cover and land-use change using multi-temporal Landsat imagery: a case study on Pisa Province in Italy. Int. J. Remote Sens. 32, 4365–4381.
Rahman, K.U., Shang, S., Zohaib, M., 2021. Assessment of Merged Satellite Precipitation Datasets in Monitoring Meteorological Drought over Pakistan. Remote Sens. (Basel) 13, 1662.
Rash, A., Mustafa, Y., Hamad, R., 2023. Quantitative assessment of Land use/land cover changes in a developing region using machine learning algorithms: A case study in the Kurdistan Region, Iraq. Heliyon 9.
Rasmussen, L.V., Rasmussen, K., Reenberg, A., Proud, S., 2012. A system dynamics approach to land use changes in agro-pastoral systems on the desert margins of Sahel. Agr. Syst. 107, 56–64.
Riaz, M.U., Raza, M.A., Saeed, A., Ahmed, M., Hussain, T., 2021. Variations in Morphological Characters and Antioxidant Potential of Different Plant Parts of Four Ziziphus Mill. Species from the Cholistan. Plants 10, 2734.
Ridd, M.K., Liu, J., 1998. A Comparison of Four Algorithms for Change Detection in an Urban Environment. Remote Sens. Environ. 63, 95–100.
Rousset, G., Despinoy, M., Schindler, K., Mangeas, M., 2021. Assessment of Deep Learning Techniques for Land Use Land Cover Classification in Southern New Caledonia. Remote Sens. (Basel) 13, 2257.
Roy, B., 2021. Optimum machine learning algorithm selection for forecasting vegetation indices: MODIS NDVI & EVI. Remote Sens. Appl.: Soc. Environ. 23, 100582.
Roy, B., Rahman, M.Z., 2023. Spatio-temporal analysis and cellular automata-based simulations of biophysical indicators under the scenario of climate change and urbanization using artificial neural network. Remote Sens. Appl.: Soc. Environ. 31, 100992.
Saleem, F., Zeng, X., Hina, S., Omer, A., 2021. Regional changes in extreme temperature records over Pakistan and their relation to Pacific variability. Atmos. Res. 250, 105407.
Salvacion, A.R., 2021. Mapping meteorological drought hazard in the Philippines using SPI and SPEI. Spat. Inf. Res. 29, 949–960.
Samie, A., Deng, X., Jia, S., Chen, D., 2017. Scenario-Based Simulation on Dynamics of Land-Use-Land-Cover Change in Punjab Province. Pakistan. Sustainability 9, 1285.
Samie, A., Abbas, A., Azeem, M.M., Hamid, S., Iqbal, M.A., Hasan, S.S., Deng, X., 2020. Examining the impacts of future land use/land cover changes on climate in Punjab province, Pakistan: implications for environmental sustainability and economic growth. Environ. Sci. Pollut. Res. 27, 25415–25433.
Sarp, G., Ozcelik, M., 2017. Water body extraction and change detection using time series: A case study of Lake Burdur, Turkey. Journal of Taibah University for Science 11, 381–391.
Schulz, J.J., Cayuela, L., Echeverria, C., Salas, J., Rey Benayas, J.M., 2010. Monitoring land cover change of the dryland forest landscape of Central Chile (1975–2008). Appl. Geogr. 30, 436–447.
Schumacher, D.L., Keune, J., Dirmeyer, P., Miralles, D.G., 2022. Drought self-propagation in drylands due to land–atmosphere feedbacks. Nat. Geosci. 15, 262–268.
Sen, P.K., 1968. Estimates of the regression coefficient based on Kendall's tau. J. Am. Stat. Assoc. 63, 1379–1389.
Shafi, A., Chen, S., Waleed, M., Sajjad, M., 2023. Leveraging machine learning and remote sensing to monitor long-term spatial-temporal wetland changes: Towards a national RAMSAR inventory in Pakistan. Appl. Geogr. 151, 102868.
Shi, L., Fan, H., Yang, L., Jiang, Y., Sun, Z., Zhang, Y., 2023. NDVI-based spatial and temporal vegetation trends and their response to precipitation and temperature changes in the Mu Us Desert from 2000 to 2019. Water Sci. Technol. 88, 430–442.
Shoba, P., Ramakrishnan, S.S., 2016. Modeling the contributing factors of desertification and evaluating their relationships to the soil degradation process through geomatic techniques. Solid Earth 7, 341–354.
Song, X.-P., Hansen, M.C., Stehman, S.V., Potapov, P.V., Tyukavina, A., Vermote, E.F., Townshend, J.R., 2018. Global land change from 1982 to 2016. Nature 560, 639–643.
Stehman, S.V., 1997. Selecting and interpreting measures of thematic classification accuracy. Remote Sens. Environ. 62, 77–89.
Tariq, A., Mumtaz, F., Majeed, M., Zeng, X., 2022. Spatio-temporal assessment of land use land cover based on trajectories and cellular automata Markov modelling and its impact on land surface temperature of Lahore district Pakistan. Environ Monit Assess 195, 114.
Thakkar, A.K., Desai, V.R., Patel, A., Potdar, M.B., 2017. Post-classification corrections in improving the classification of Land Use/Land Cover of arid region using RS and GIS: The case of Arjuni watershed, Gujarat, India. Egypt. J. Remote Sens. Space Sci. 20, 79–89.
Tucker, C.J., 1979. Red and photographic infrared linear combinations for monitoring vegetation. Remote Sens. Environ. 8, 127–150.
Ullah, I., Ma, X., Yin, J., Asfaw, T.G., Azam, K., Syed, S., Liu, M., Arshad, M., Shahzaman, M., 2021. Evaluating the meteorological drought characteristics over Pakistan using in situ observations and reanalysis products. Int. J. Climatol. 41, 4437–4459.
Ullah, I., Ma, X., Yin, J., Saleem, F., Syed, S., Omer, A., Habtemicheal, B.A., Liu, M., Arshad, M., 2022. Observed changes in seasonal drought characteristics and their possible potential drivers over Pakistan. Int. J. Climatol. 42, 1576–1596.
Wahla, S.S., Kazmi, J.H., Tariq, A., 2023. Mapping and monitoring of spatio-temporal land use and land cover changes and relationship with normalized satellite indices and driving factors. Geology, Ecology, and Landscapes 1–17.
Waleed, M., Sajjad, M., Shazil, M.S., Tariq, M., Alam, M.T., 2023. Machine learning-based spatial-temporal assessment and change transition analysis of wetlands: An application of Google Earth Engine in Sylhet, Bangladesh (1985–2022). Eco. Inform. 75, 102075.
Wang, W., Chen, Y., Wang, W., Yang, Y., Hou, Y., Zhang, S., Zhu, Z., 2022. Assessing the Influences of Land Use Change on Groundwater Hydrochemistry in an Oasis-Desert Region of Central Asia. Water 14, 651.
Wang, H., Liu, Y., Wang, Y., Yao, Y., Wang, C., 2023. Land cover change in global drylands: A review. Sci. Total Environ. 863, 160943.
Wang, Z., Wu, B., Ma, Z., Zhang, M., Zeng, H., 2024. Distinguishing natural and anthropogenic contributions to biological soil crust distribution in China's drylands. Sci. Total Environ. 907, 168009.
Wardhani, N.W.S., Rochayani, M.Y., Iriany, A., Sulistyono, A.D., Lestantyo, P., 2019. Cross-validation Metrics for Evaluating Classification Performance on Imbalanced Data. In: 2019 International Conference on Computer, Control, Informatics and Its Applications (IC3INA), pp. 14–18.
Xiao, J., Shen, Y., Tateishi, R., Bayaer, W., 2006. Development of topsoil grain size index for monitoring desertification in arid land using remote sensing. Int. J. Remote Sens. 27, 2411–2422.
Xie, L., Wang, H., Liu, S., 2022. The ecosystem service values simulation and driving force analysis based on land use/land cover: A case study in inland rivers in arid areas of the Aksu River Basin. China. Ecological Indicators 138, 108828.
Yamaki, S., Seki, S., Sugita, N., Yoshizawa, M., 2021. Performance Evaluation of Cross Correlation Functions Based on Correlation Filters, 2021 20th International Symposium on Communications and Information Technologies (ISCIT), pp. 145-149.
Yang, Q., Ma, Z., Zheng, Z., Duan, Y., 2017. Sensitivity of potential evapotranspiration estimation to the Thornthwaite and Penman-Monteith methods in the study of global drylands. Adv. Atmos. Sci. 34, 1381–1394.
Zhao, Y., Chang, C., Zhou, X., Zhang, G., Wang, J., 2024. Land use significantly improved grassland degradation and desertification states in China over the last two decades. J. Environ. Manage. 349, 119419.
Zubair, M., Saleem, A., Baig, M.A., Islam, M., Razzaq, A., Gul, S., Ahmad, S., Moyo, H.P., Hassan, S., Rischkowsky, B., Ibrahim, M.N.M., Louhaichi, M., 2018. The Influence of Protection From Grazing on Cholistan Desert Vegetation, Pakistan. Rangelands 40, 136–145.